ORGANIC PROCESS RESEARCH & DEVELOPMENT
OPR&D

pubs.acs.org/OPRD

Article

Development of a Green and Sustainable Manufacturing Process for Gefapixant Citrate (MK-7264) Part 3: Development of a One-Pot Formylation−Cyclization Sequence to the Diaminopyrimidine Core

Kallol Basu,* Dan Lehnherr,* Gary E. Martin, Richard A. Desmond, Yu-hong Lam, Feng Peng, John Y. L. Chung, Rebecca A. Arvary, Michael A. Zompa, Si-Wei Zhang, Jinchu Liu, Zachary E. X. Dance, Patrick Larpent, Ryan D. Cohen, Francisco J. Guzman, Nicholas J. Rogus, Michael J. Di Maso, Hong Ren, and Kevin M. Maloney

Cite This: https://dx.doi.org/10.1021/acs.oprd.0c00246

Read Online

ACCESS | Metrics & More | Article Recommendations | Supporting Information

ABSTRACT: The development of a safe, robust, and efficient manufacturing route for the synthesis of diaminopyrimidine **1**, a key intermediate to gefapixant citrate (MK-7264), is described. A full mechanistic understanding of the cyclization step in the presence of guanidine was established by performing isotopic labeling experiments and identification of impurities. Guided by the mechanistic understanding, further attempts to modify the cyclization reaction by employing additives to reduce the triazine (**9**) formation and guanidine loading will also be presented. This newly developed method delivered compound **1** in 88−94% yield on a commercial scale and addressed the shortcomings of the early synthetic route including high PMI, low atom economy, long cycle-time, and multiple purifications to achieve the desired quality.

KEYWORDS: *cyclization, heterocycle, pyrimidine, triazine, process optimization, reaction mechanism*

INTRODUCTION

Diaminopyrimidine **1** represents the penultimate intermediate toward the synthesis of gefapixant citrate (MK-7264), a first-in-class P2X3 antagonist currently in phase 3 clinical trials for chronic cough.[1] The synthetic route for compound **1** developed by Afferent[2] is depicted in Scheme 1. Sequential treatment of cyanomethyl ether (CME) **2** with *tert*-butoxybis(dimethylamino)methane (Bredereck's reagent)[3] and aniline hydrochloride produced enamine **3**, which underwent condensation with guanidine carbonate (**G·0.5H$_2$CO$_3$**) to produce desired compound **1**. While this protocol was utilized to synthesize kilogram quantities of diaminopyrimidine **1**, a number of factors rendered this approach unsuitable as the long-term supply route capable of delivering metric ton quantities of intermediate **1**. For example, the high price (> $1700/kg)[4] and long lead-time of Bredereck's reagent on scale made usage of this reagent unfeasible. Use of aniline hydrochloride for the formation of the enamine not only resulted in poor atom economy but also produced aniline-related potential genotoxic impurities; consequently, multiple crystallizations were required to obtain the desired purity level of compound **1**. Additionally, an aqueous workup of intermediate enamine **3** (using toluene−water), followed by distillation to reduce the water content, was required prior to it being used in the cyclization step with guanidine carbonate to generate product **1**. Collectively, these liabilities contributed to long cycle times (∼4 days for reaction time only), modest yields (55−60% over 3 steps), and high process mass intensity[5,6] (step-PMI = 88 normalized to 1 kg of **1**), precluding the implementation of this route as a long-term solution. It became clear that a superior synthetic approach was required to enable the team to provide significant quantities of diaminopyrimidine **1** to meet the active pharmaceutical ingredient demand for phase 3 clinical studies and form the basis of a viable manufacturing process.

RESULTS AND DISCUSSION

Alkylation of Phenol—A Reaction Stream for the Pyrimidine Cyclization Step. In order to synthesize pyrimidine **1**, we first needed to develop a safe and robust process to alkylate phenol **4** and generate pyrimidine starting material **2**.[7] Earlier deliveries of CME **2** relied on an alkylation process of phenol **4**, in which chloroacetonitrile was added to a mixture of KOH and dimethyl sulfoxide (DMSO) at high temperature (Scheme 1). This approach was deemed unacceptable because of the process safety risks (an uncontrolled exotherm) associated with the decomposition of DMSO under these conditions.[8] An initial screening of solvents indicated that *N*-methyl-2-pyrrolidone (NMP) was an effective and safe replacement for DMSO, so we undertook an examination of alkylation conditions in this solvent.[9] A high-level summary of various alkylation conditions to generate CME **2** is provided in Table 1. A survey of the alkali *tert*-butoxides initially suggested

Received: May 22, 2020

Scheme 1. First-Generation Route to Diaminopyrimidine 1

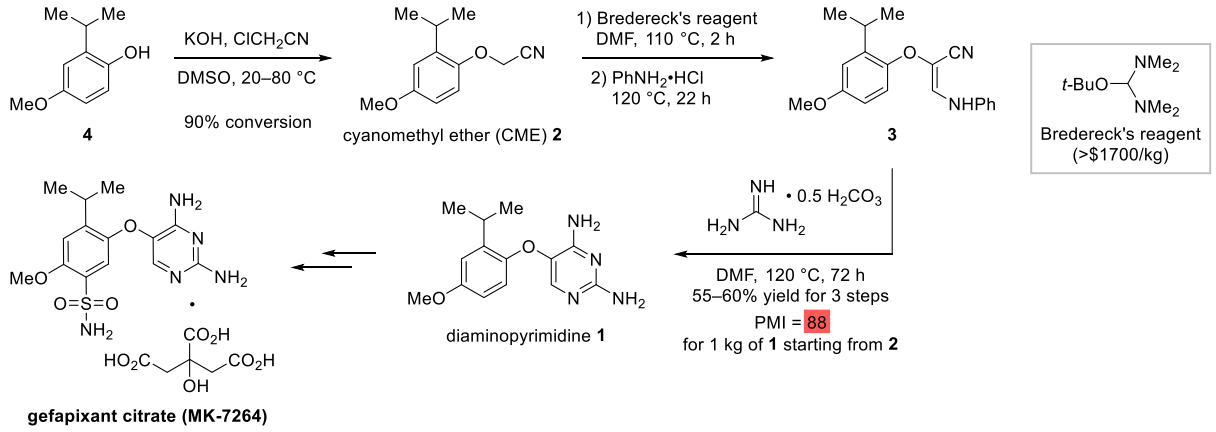

Table 1. Optimization of Phenol Alkylation to Generate CME 2

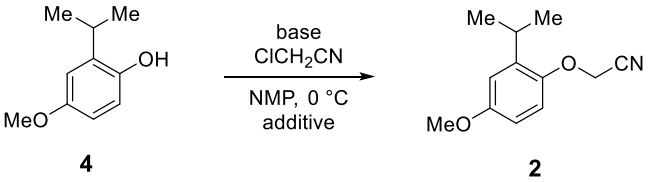

entry	base	additive	conversion (%)
1	KO*t*-Bu		73
2	NaO*t*-Bu		81
3	LiO*t*-Bu (lot 1)		>99
4	LiO*t*-Bu (lot 2)		88
5	LiO*t*-Bu (lot 2)	10 wt % H_2O[a]	>99
6	LiOH		70
7	LiOH	10 wt % H_2O[a]	>99
8	NaO*t*-Bu	10 wt % H_2O[a]	>99
9	KO*t*-Bu	10 wt % H_2O[a]	>99
10	50 wt % NaOH		>99
11[b]	**50 wt % NaOH**		**>99 (97%)**[c]

[a]10 wt % H_2O is with respect to phenol **4**. [b]Run in 5 volumes NMP and 1 volume of toluene. [c]Assay yield.

that the identity of the base may be important, where smaller cations improved the outcome (Table 1, entries 1−3). However, upon further inspection of different lots of LiO*t*-Bu, we postulated that the additional conversion was arising from adventitious amounts of water (entry 3 vs 4). Indeed, when we spiked our reactions with water (10 wt % with respect to phenol **4**), not only were we able to obtain comparable results with different lots of LiO*t*-Bu (entry 5) but also, more importantly, with all of the bases performed identically (entries 6−9). This result led us to conduct the reaction with inexpensive and easily handled aqueous solutions of sodium hydroxide as the base. Employing these conditions led to full conversion to the desired CME **2**. The results shown in Table 1 when using 10 wt % water demonstrates that hydroxide is the active base for this transformation. The stronger *tert*-butoxide base is thought to decompose chloroacetonitrile at a competitive rate relative to that of the desired alkylation. The effect of adding water to the lithium hydroxide reaction (entry 7) provides a homogeneous reaction mixture and eliminates any sensitivities to mass transfer. With an eye toward telescoping the incoming stream of methoxyphenol in toluene, we explored mixtures of NMP and toluene for the formation of CME **2**. A 5:1 mixture of NMP/toluene (entry 11) provided comparable results to the NMP conditions (entry 10). A key amide impurity was found to form when the ratio of NMP/toluene was less than 4:1. The 5:1 NMP/toluene conditions provided end of reaction (EOR) stability for >72 h and could be safely scaled up to deliver hundreds of kilograms of compound **2** without experiencing any safety-related issues. This discovery allowed us to telescope the methoxyphenol stream isolated from the upstream methoxylation reaction[10] directly into the alkylation reaction without the need for extensive solvent switching. An aqueous workup provided compound **2** as a solution in toluene that could be distilled to the appropriate volume for use in the pyrimidine-forming reaction.

Cyclization of CME to Diaminopyrimidine—Exploring Alternatives to Bredereck's Reagent. Seeking to avoid the use of Bredereck's reagent and aniline hydrochloride, initial efforts toward improving the pyrimidine formation were targeted toward the use of *N*,*N*-dimethylformamide (DMF)−DMA,[3] a lower-cost alternative for the synthesis of an enamine intermediate analogous to compound **3**. To our surprise, treatment of CME **2** with DMF−DMA in polar aprotic solvents resulted only in unreacted CME **2**, with no trace of the enamine intermediate. This observation was supported by density functional theory (DFT) calculations (Scheme 2) predicting an exergonicity of 7.0 kcal/mol for the synthesis of enamine **5a** using Bredereck's reagent (eq 1) but an endergonicity of 1.5 kcal/mol for the analogous synthesis using DMF−DMA (eq 2). Prompted by the DFT prediction that the exchange of a methoxy group of DMF-DMA by pyrrolidine was slightly exergonic (eq 3), we posited that a Bredereck-like intermediate could be formed *in situ* by mixing DMF−DMA and a secondary amine at elevated temperatures. In addition, calculations (eq 4) predicted a thermodynamically downhill process for the formation of enamines **5b** and **5e** when pyrrolidine or azetidine were used as additives. Conversely, the use of diisopropylamine or piperidine was predicted to be ineffective based on the positive Gibbs energies of reaction for the formation of intermediates **5c** and **5d**, respectively. Thus, because of the lower cost of pyrrolidine, we decided to investigate the combination of DMF−DMA and pyrrolidine toward the formation of intermediate enamine and subsequent cyclization reaction (Scheme 3). Gratifyingly, heating a mixture of CME **2**, DMF−DMA, and pyrrolidine in DMF produced enamine **5b**, which, following an aqueous wash, smoothly underwent cyclization with guanidine to afford the desired diaminopyrimidine in modest yield (75%). Encouraged by this initial result,

https://dx.doi.org/10.1021/acs.oprd.0c00246
Org. Process Res. Dev. XXXX, XXX, XXX−XXX

Scheme 2. DFT-Computed Thermodynamics for Alternatives to Bredereck's Reagent[11]

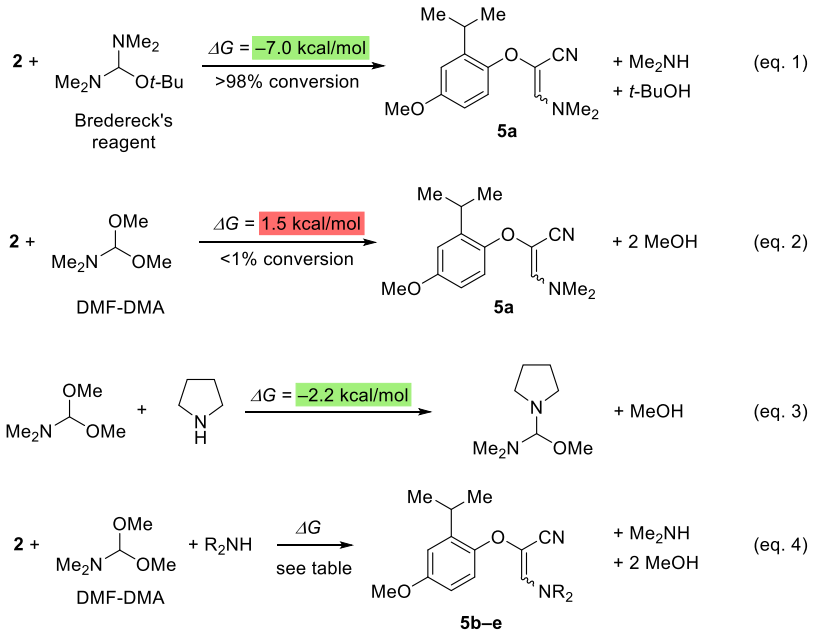

Scheme 3. Synthesis of the Diaminopyrimidine Core Employing DMF−DMA and Pyrrolidine as an Alternative to Bredereck's Reagent

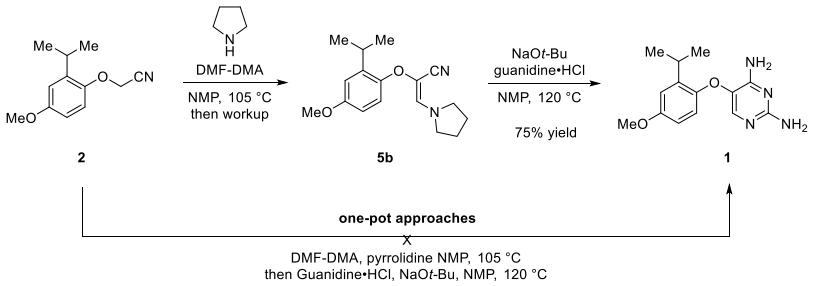

Scheme 4. Retrosynthetic Strategy for the Second-Generation Synthesis

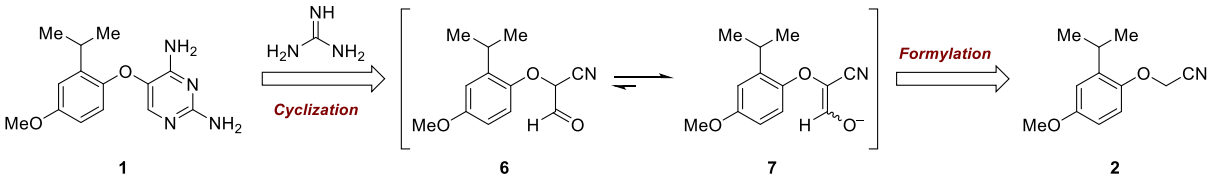

we investigated a one-pot approach; unfortunately, all our attempts to directly cyclize the enamine with guanidine under these conditions failed to produce any desired product. While this approach served as proof-of-concept toward an alternative to expensive Bredereck's reagent, the need for an additional aqueous workup of the enamine intermediate prior to the cyclization step, combined with a modest isolated yield, forced us to evaluate other strategies for formation of the diaminopyrimidine core.

Second-Generation Synthesis Approach. Undaunted by the failure of the through-process shown in Scheme 3, we continued to explore alternative methods for synthesis of the diaminopyrimidine[12] moiety utilizing inexpensive and readily available reagents. As shown in Scheme 4, we hypothesized that the diaminopyrimidine moiety could be synthesized via a condensation reaction between cyanoaldehyde **6** and guanidine. In the forward sense, we envisioned that the formation of enolate **7** via a base-mediated formylation of compound **2**, followed by cyclization with guanidine, would afford the key intermediate **1**.

https://dx.doi.org/10.1021/acs.oprd.0c00246
Org. Process Res. Dev. XXXX, XXX, XXX−XXX

Scheme 5. Importance of Order of Addition toward Minimizing the CME Dimer in Enolate Formation

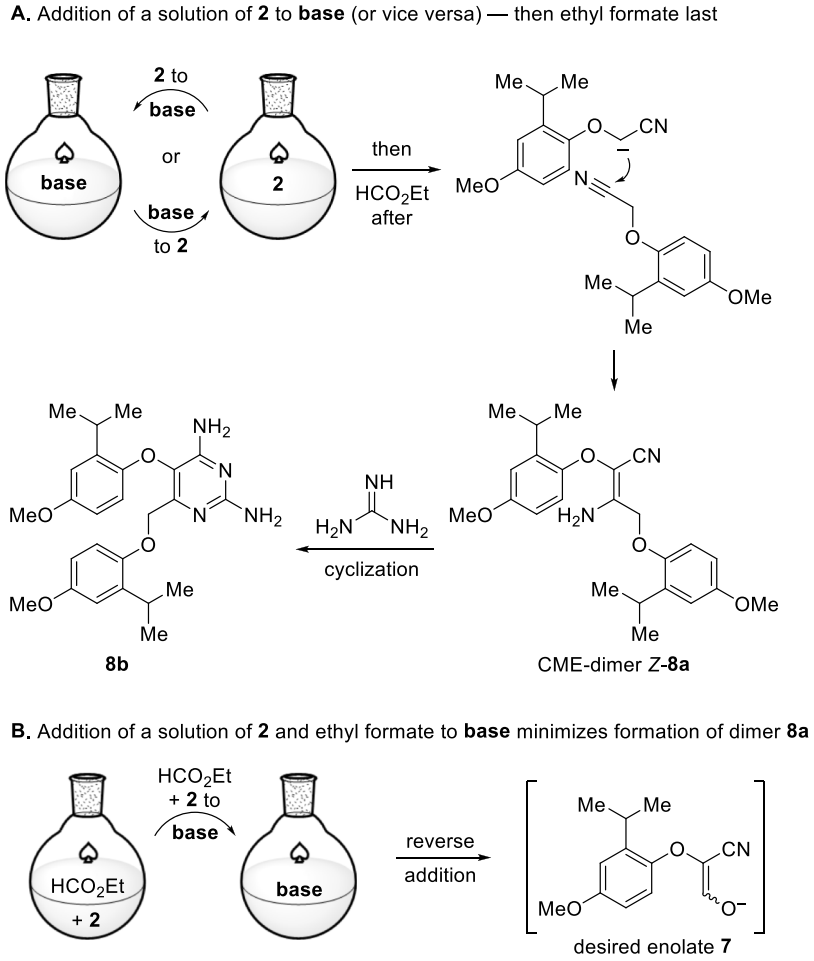

Table 2. Optimization of Enolate Formation

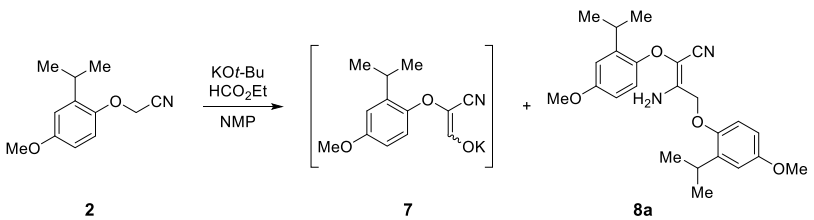

entry	KO*t*-Bu (equiv)	HCO_2Et (equiv)	7 (LCAP)[a]	8a (LCAP)[a]	2 (LCAP)[a]
1	1.00	2.00	76.0	1.1	19.9
2	1.25	2.00	86.8	1.5	10.0
3	1.50	2.00	93.9	1.5	3.7
4	1.75	2.00	96.1	1.5	1.8
5	2.00	2.00	98.1	1.2	0.2
6	**2.25**	**2.00**	**98.5**	**1.0**	**0.0**
7	2.25	1.00	70.7	26.3	0.0
8	2.25	1.25	75.3	22.2	0.0
9	2.25	1.50	95.4	3.6	0.0
10	2.25	1.75	97.9	1.2	0.0

[a]Area % by HPLC at EOR.

If successful, this strategy would represent a straightforward and atom-economical process.

As a proof-of-concept, we first evaluated the formation of enolate **7** by following literature precedent.[13] All our initial attempts to deprotonate compound **2** and quench the ensuing anion with ethyl formate resulted in exclusive formation of the CME dimer **8a** (Scheme 5A). While several examples of generating enolates using ethyl formate as the formyl source in the presence of a base (e.g., NaH and NaOEt) are known in the literature;[5] to the best of our knowledge, no example has been

https://dx.doi.org/10.1021/acs.oprd.0c00246
Org. Process Res. Dev. XXXX, XXX, XXX−XXX

Scheme 6. Balanced Equation for CO Generation during Enolate Formation

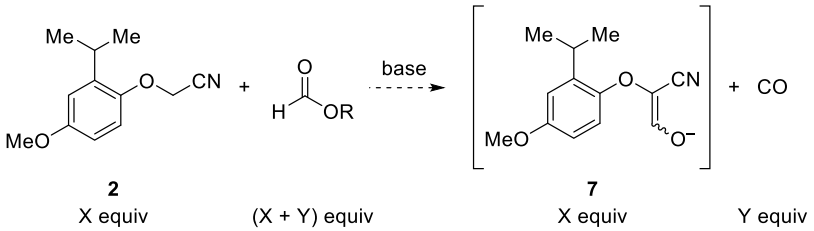

reported starting from a CME derivative. The presence of an oxygen atom at the β-position with respect to the nitrile not only decreases the acidity of the α-methylene protons but also enhances the reactivity of the resulting anion; therefore, in the absence of an alkylating agent, the anion intermediate immediately reacts with a molecule of starting material **2**, resulting in the exclusive formation of CME dimer **8a**.

Minimizing the dimerization of CME during enolate formation is critical for two reasons: (1) formation of CME dimer **8a** negatively impacts the yield of enolate **7** and, thus, the yield of product **1**; and (2) CME dimer **8a** reacts with guanidine during the cyclization step, leading to impurity **8b**, which is difficult to reject during the isolation of compound **1**. After substantial experimentation, it was discovered that the formation of dimer **8a** could be suppressed by reverse addition of a solution containing both compound **2** and ethyl formate to a solution of the base (Scheme 5B). Under this protocol, formation of the desired enolate **7** became the major pathway.

Employing this effective order of addition (Scheme 5B), a large number of experiments were carried out to better understand the enolate formation by screening solvent, base, and temperature, and the results are summarized as follows: (1) polar aprotic solvents (NMP, dimethylacetamide, and DMF) are superior solvents, ethereal solvents (tetrahydrofuran) tend to produce more CME dimer **8a**, while alcohol solvents (EtOH, MeOH, and *i*-PrOH) proved unproductive; (2) strong, non-nucleophilic bases (KO*t*-Bu, NaO*t*-Bu, KHMDS, and KO*t*-amyl) are required for deprotonation, while use of slightly weaker bases (KOEt and NaOEt) results in incomplete reactions and more CME dimer formation; (3) the potassium counter ion is critical to clean conversion of CME **2** to enolate **7**; (4) a cleaner reaction profile was observed at lower temperature (−20 to 0 °C), while elevated temperature (20 to 30 °C) results in a higher amount of CME dimer formation [3−4 high-performance liquid chromatography (HPLC) area %]. Considering availability and low cost at a commercial scale, we decided to perform the enolate formation in NMP with *t*-BuOK as the base and ethyl formate as the formylating agent.

Enolate Formation. With an understanding of the order of addition and the nature of reagents in hand, we began evaluating the effect of base and ethyl formate stoichiometry to further optimize the enolate formation at −10 to 0 °C (Table 2). Initial experiments with a lower amount of base (entries 1 and 2) afforded incomplete conversion and a substantial amount of unreacted CME **2**. This result was attributed to the ineffectiveness of potassium ethoxide, formed during enolate generation, as a base to drive the formation of enolate **7**. The conversion became more favorable as the amount of the starting base was increased to 2.0 equiv (entries 3, 4, and 5). In contrast, experiments employing a lower amount of ethyl formate led to the formation of a higher amount of the CME dimer (entries 7 and 8), presumably due to high intrinsic reactivity of the anion derived from CME **2** in the absence of an adequate amount of ethyl formate. Gratifyingly, when the amount of ethyl formate was increased to 1.5 and 1.75 equiv (entries 9 and 10), the productive pathway was favored, resulting in >95% target enolate and 3.6 and 1.3 area % of the CME dimer, respectively. Knowing the intrinsic reactivity of the CME anion could pose a challenge upon scaling up, we decided to perform the enolate formation in the presence of 2.0 equiv of ethyl formate and 2.25 equiv of base (entry 6), which resulted in ≤1 area % of the CME dimer, with no observable unreacted CME **2**.

Safety assessment showed that the total adiabatic temperature increase (ΔT_{ad}) for the entire enolate formation involves moderate exotherm with a ΔT_{ad} of ∼34 K. Closed tube differential scanning calorimetry data suggest that an exotherm of 37 J/g is released at an initiation temperature of 122 °C. These data were in line with established safety considerations for scale-up.[14] However, during optimization, off-gassing was observed when a mixture of CME **2** and ethyl formate was added to the solution of potassium *tert*-butoxide. As a result, we carried out an experiment to evaluate the stability of ethyl formate alone in the presence of the base and noticed a similar off-gassing event, which prompted us to hypothesize a decomposition pathway of ethyl formate in the presence of the base. While the gas evolution event was mentioned by Myers and co-workers,[15] no additional information was provided. This competing decomposition pathway also explains why excess of ethyl formate (2.0 equiv) is needed to successfully convert all CME **2** to enolate **7**.

We employed process analytical technology to conduct the enolate formation in the presence of both solution and headspace Fourier-transform infrared spectroscopy (FT-IR) probes to understand the type of gas released and the rate of off-gassing, which provided three key pieces of information: (1) the gas evolved during the enolate formation was carbon monoxide; (2) the rate of CO off-gassing was directly proportional to the addition rate of a mixture of ethyl formate and CME **2** to the base solution, and the off-gassing stops immediately when the addition is stopped; (3) accurate calibration allowed excellent quantification of CO emission, which was consistent with the theoretical prediction shown in Scheme 6. Furthermore, the *in situ* solution FT-IR spectrum revealed no trace of ethyl formate throughout the addition, which was also confirmed via gas chromatography (GC) analysis of the final enolate solution, indicating its rapid and complete consumption under these reaction conditions. These important pieces of data enabled us to determine the required rate of addition during the enolate formation. This information is critical because the amount of CO formed can be easily calculated based on ethyl formate charge, which would help us to determine the addition time to control the rate of CO evolution. As illustrated in Scheme 6, one equivalent of ethyl formate is used toward enolate formation for

https://dx.doi.org/10.1021/acs.oprd.0c00246
Org. Process Res. Dev. XXXX, XXX, XXX−XXX

one equivalent of CME **2**, while the remaining ethyl formate decomposes to form CO.

Based on the balanced equation above, in which the amount of CO directly related to the amount of ethyl formate is utilized in the enolate formation, we realized that the local CO emission guidelines would limit material throughput in the absence of any engineering control such as a thermal oxidizer unit (TOU). For example, for 50 kg of CME **2** (244 mol), 15 pounds of CO (244 mol) would be generated during the enolate formation under the optimized conditions employing 2.0 equiv of ethyl formate (488 mol); therefore, the addition time can be adjusted to 4 h to maintain CO release under the local limit of 4 lb/h (~1.8 kg/h). In order to maintain CO emission in check during the enolate formation in the absence of a TOU, larger-scale batches would require longer addition times (e.g., enolate formation for 250 kg of CME **2** would require addition of reagents over a period of ~40 h). We explored whether enolate formation and subsequent cyclization could tolerate such a long aging process, and, indeed, compound **1** was still generated in high yield and good quality. Ultimately, we did not have to rely on such a long addition time, as alternative engineering controls (i.e., a TOU) enabled us to bypass this concern, which rendered the enolate formation operationally feasible within 8−10 h, irrespective of the starting quantity of CME **2**.[16]

Cyclization Reaction. After establishing the enolate formation with KO*t*-Bu (2.25 equiv) and ethyl formate (2.0 equiv) in NMP, we turned our attention to the cyclization reaction by directly charging guanidine salt to the enolate solution and subsequently heating to 115 °C for 12−15 h. To our surprise, reactions using 3.0 equiv of guanidine carbonate (**G·0.5H$_2$CO$_3$**) (as was done in the first-generation synthesis) performed poorly, leading to incomplete reaction even after prolonged heating (~30 HPLC area % enolate left). We screened a variety of readily available guanidine salts for the cyclization step and collected time-course data (Figure 1). The

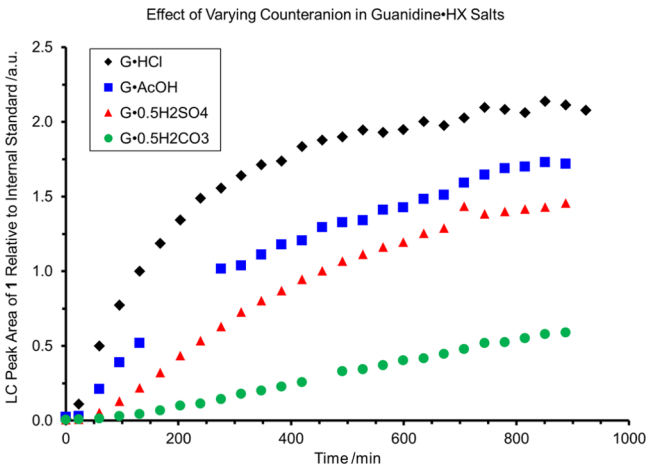

Figure 1. Temporal profile for the formation of diaminopyrimidine **1** using various guanidine salts (3 equiv relative to compound **2**) illustrating the improved kinetics with **G·HCl**.

temporal data in Figure 1 clearly highlight the improved rate of product formation when utilizing guanidine HCl (**G·HCl**) in comparison to other guanidine salts such as guanidine acetate (**G·AcOH**), guanidine sulfate (**G·0.5H$_2$SO$_4$**), and guanidine carbonate (**G·0.5H$_2$CO$_3$**). These data also highlight that **G·0.5H$_2$CO$_3$**, used in the original process, is the slowest at forming product **1**. This finding led us to focus on developing the cyclization of the enolate with **G·HCl**, which provides complete conversion of enolate and an acceptable reaction profile after 15 h of heating at 115 °C.

Initial cyclization reactions involving 2.0 equiv of **G·HCl** at 115 °C for 15 h resulted in full conversion of enolate, delivering 75 HPLC area % of the desired diaminopyrimidine **1** at the end of the reaction (Table 3, entry 1). One of the key identifiable

Table 3. Effect of the Guanidine Hydrochloride Amount in Cyclization Reaction

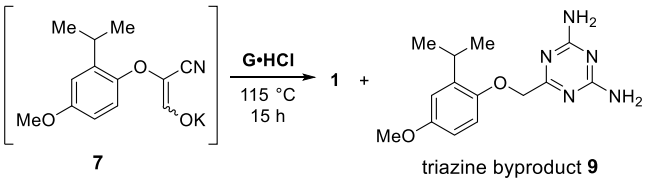

7 triazine byproduct **9**

entry	guanidine	charge	**1** (LCAP)[a]	**9** (LCAP)[a]
1	2.0	equiv	75.0	11.1
2	3.0	equiv	87.2	6.6
3	4.5	equiv	89.5	4.9
4	6.0	equiv	92.0	3.1
5	**8.0**	**equiv**	**93.5**	**2.1**

[a]Area % by HPLC at EOR.

components of the mass balance of this cyclization reaction was triazine **9**, whose structure was determined through extensive NMR spectroscopic and mass spectrometric analysis on a purified sample of this compound. While variation of temperature and dilution did not afford any significant advantage, the number of equivalents of **G·HCl** used proved a critical parameter for reaction performance and optimization (Table 3). For instance, when the amount of **G·HCl** was increased from 2.0 to 3.0 equiv, the amount of triazine at the end of the reaction dropped from 11.1 to 6.6 HPLC area %, while improving the diaminopyrimidine liquid chromatography area percent (LCAP) to 87.2%. It became apparent that, with the increase of guanidine amount, the conversion to the desired product continues to improve while simultaneously decreasing the triazine formation.

With the aim to further understand the cyclization reaction, an investigation into the reaction kinetics was undertaken. Varying the initial concentration of **G·HCl**, while maintaining all other reaction parameters identical, revealed that the rate of the cyclization reaction is first order in **G·HCl** (Figure 2). The reaction with 2.5 equiv of **G·HCl** proved to be sluggish; however, significant rate acceleration was observed with 7.5 equiv of **G·HCl**, resulting in complete consumption of enolate within 4 h and less of impurity **9**. On the basis of this observation, we hypothesized that increasing the amount of guanidine during the course of cyclization would maximize the yield of compound **1** by favoring the productive pathway while minimizing the side reactions, leading to the formation of triazine **9**. We note that performing the cyclization at temperatures lower than 115 °C (e.g. 95 or 105 °C) resulted in significantly slower cyclization rates, which resulted in longer reaction times and incomplete consumption of enolate.

Mechanism and Isotopic Labeling Studies. While the isolation of diaminopyrimidine **1** was achieved in high yield and purity on laboratory scale, the question regarding why high amounts (8 equiv) of **G·HCl** were required to achieve these results remained unanswered. We designed a series of isotopic

https://dx.doi.org/10.1021/acs.oprd.0c00246
Org. Process Res. Dev. XXXX, XXX, XXX−XXX

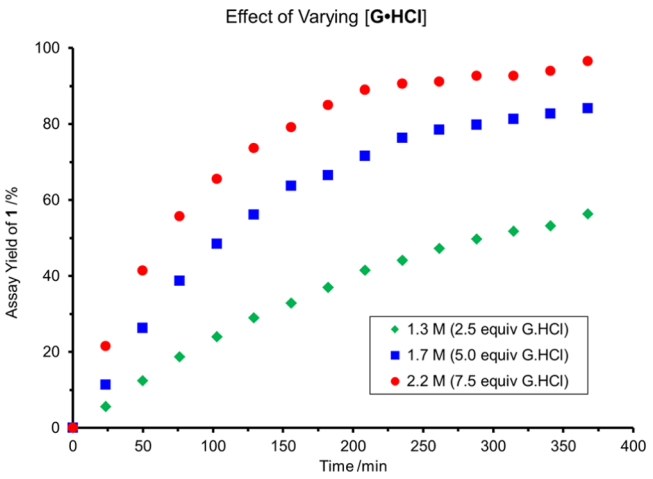

Figure 2. Temporal data for the formation of product **1** using varying concentrations of **G·HCl** (1.3, 1.7, and 2.2 M), illustrating the positive order dependence.

labeling experiments aimed at gaining further mechanistic insight into the cyclization in order to apply this information toward designing an improved cyclization process (e.g., using less **G·HCl** while minimizing the amount of triazine **9** impurity). These isotopic labeling experiments were designed to track the incorporation, or lack thereof, of either ^{13}C or ^{15}N isotopic labels into specific locations in the desired product and the triazine formed, depending on the choice of the isotopically labeled starting material (Scheme 7). In all cases, both the desired product and the triazine were isolated via purification, and extensive NMR and high-resolution mass spectrometry experiments provided isotopic incorporation results and unequivocal structural verification.

Scheme 7A illustrates the preparation of the enolate from CME **2** using ^{13}C-labeled ethyl formate and its reaction with 3 equiv of **G·HCl**. This reaction led to formation of the desired diaminopyrimidine containing a ^{13}C at the C-6 position. In contrast, no evidence of incorporation of the ^{13}C label from ethyl formate was observed in triazine samples. These data are consistent with loss of the −CHO group from enolate during the formation of triazine. When a similar experiment was carried out using ^{15}N-labeled CME **2** (Scheme 7B), the desired product contained ^{15}N at the expected amino group on C-4, while no evidence of incorporation of the ^{15}N label in the triazine was observed. These data suggest the loss of nitrogen from the nitrile group of CME **2** during the formation of triazine. Finally, cyclization of the enolate with ^{13}C-labeled **G·HCl** led to the formation of desired diaminopyrimidine samples containing a ^{13}C-label at the C-2 position as expected, while both C-2 and C-4 positions in the triazine had incorporation of a ^{13}C-label (Scheme 7C). We hypothesized that an equilibrium between guanidine and biguanide (**BG**) is established under the cyclization conditions (*vide infra*), where the latter is responsible for the formation of triazine **9**. Based on the results from labeling experiments, we have proposed a reaction pathway that results in

Scheme 7. Isotopic Labeling Experiments

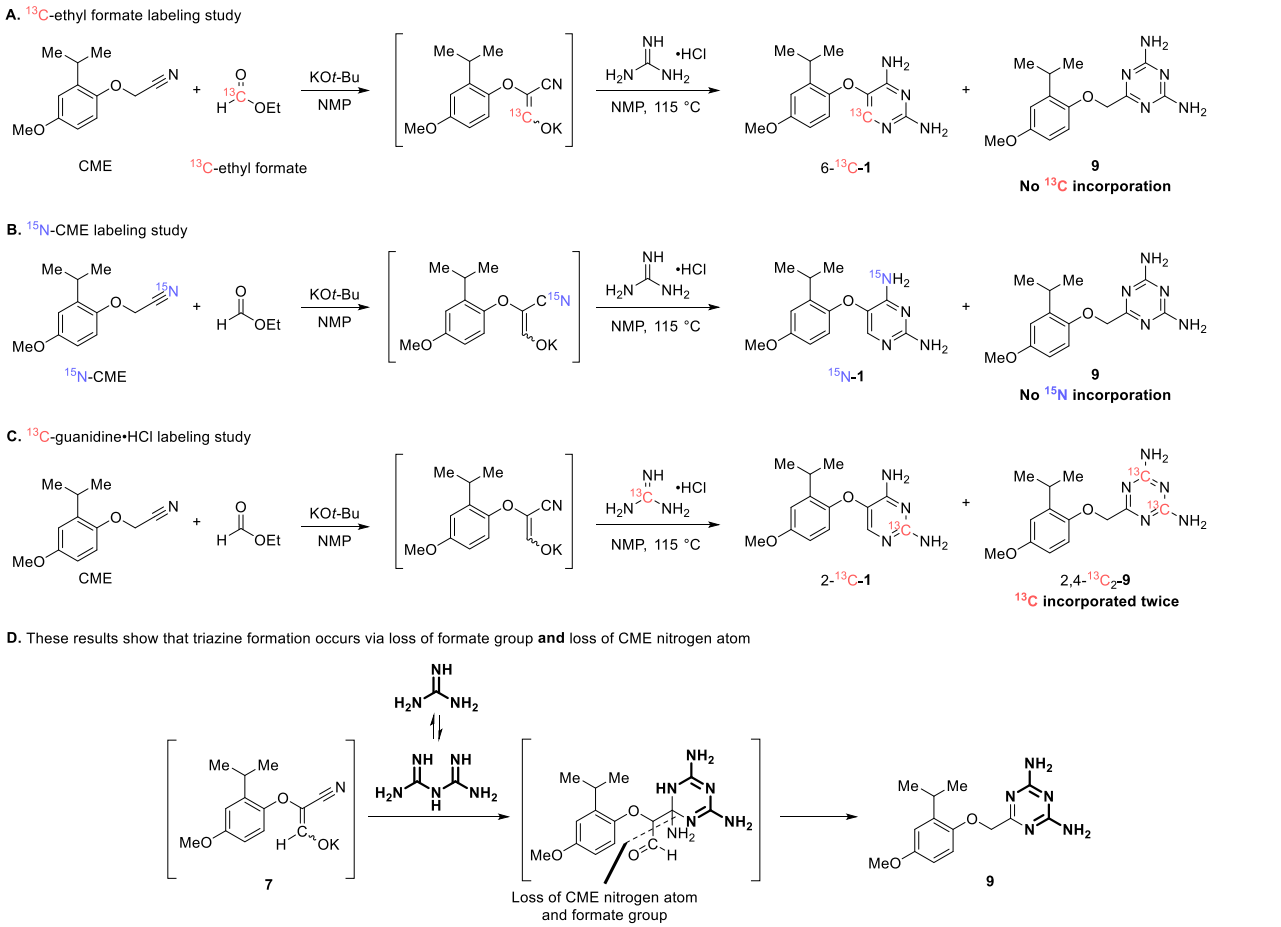

https://dx.doi.org/10.1021/acs.oprd.0c00246
Org. Process Res. Dev. XXXX, XXX, XXX−XXX

the loss of a nitrogen and a carbon atom from the enolate, potentially via the intermediate shown in Scheme 7D.[17]

In order to investigate whether the enolate can react with **BG·HCl** to generate triazine, a series of experiments were performed, and the corresponding data are summarized in Table 4. To our surprise, when freshly prepared enolate

Table 4. Partitioning of Products 1 and 9 When Reacting Enolate 7 with Varying Ratios of G·HCl and BG·HCl

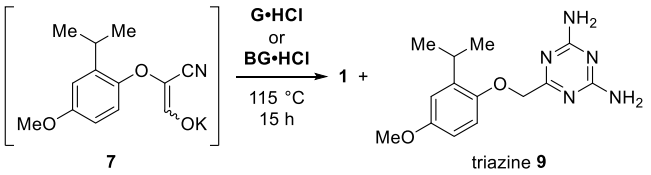

entry	equivalents of 7	G·HCl	BG·HCl	1:9[a]
1	1		3	1.9:1
2	1		6	1.3:1
3	1		9	1.2:1
4	1	3	3	4.5:1
5	1	3	6	3.6:1
6	1	3	9	3.3:1

[a]Based on area % by HPLC at EOR.

solutions were heated with varying amounts of **BG·HCl** at 115 °C for 15 h (entries 1−3), both compounds **1** and **9** were formed. The observation that desired **1** is also formed suggests that guanidine is reversibly generated from biguanide under the cyclization conditions. Interestingly, the ratio of **1** to **9** decreases as the ratio of **G·HCl** to **BG·HCl** was changed from 1:1 (entry 4) to 1:3 (entry 6). Compound **1** was always preferentially generated, irrespective of the ratio of reagents used, suggesting a lower activation barrier in the cyclization reaction with guanidine as compared to that with biguanide.

It became imperative to investigate how biguanide is formed from guanidine. In the balanced reaction converting CME **2** to the enolate, excess alkoxide (likely in the form of ethoxide) and alcohol (*t*-BuOH and EtOH) are present (Scheme 8A). Heating **G·HCl** alone in NMP overnight did not result in conversion to **BG**, and, analogously, heating **BG·HCl** did not result in the formation of **G** (Scheme 8B).

In order to determine whether **G·HCl** could produce **BG** in the presence of alcohols or alkoxides, we independently heated mixtures of **G·HCl** and alkoxides (or alcohols) in varying ratios at 115 °C in NMP overnight in sealed microwave vials to mimic reaction conditions (Scheme 8C). These stress tests clearly showed the formation of biguanide when **G·HCl** was exposed to alkoxides (KO*t*-Bu or KOEt) but not in the presence of alcohols (*t*-BuOH or EtOH), as determined by HPLC. A similar stress test of **BG·HCl** in NMP at 115 °C overnight in the presence of either alkoxides (KO*t*-Bu or KOEt) or alcohols (*t*-BuOH or EtOH) demonstrated that only alkoxides were capable of promoting the generation of guanidine. These key experiments clearly established the role of alkoxides in the formation of biguanide from guanidine during the cyclization.

A plausible mechanism to generate biguanide in the presence of alkoxide is via an isourea[18] intermediate, which, in turn, undergoes substitution by another molecule of guanidine (Scheme 9).[19] Both the addition of alkoxides to guanidine to

Scheme 9. Illustration of a Potential Pathway to Convert Guanidine (G) to Biguanide (BG) via Isourea

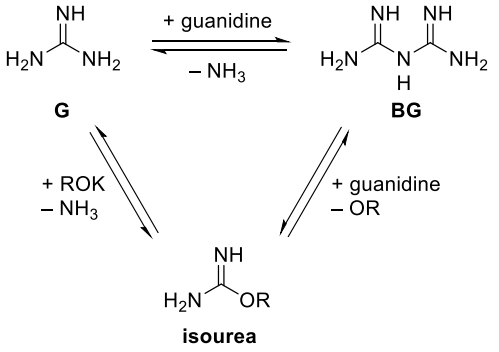

Scheme 8. Illustration of Conditions That Can and Cannot Interconvert G and BG

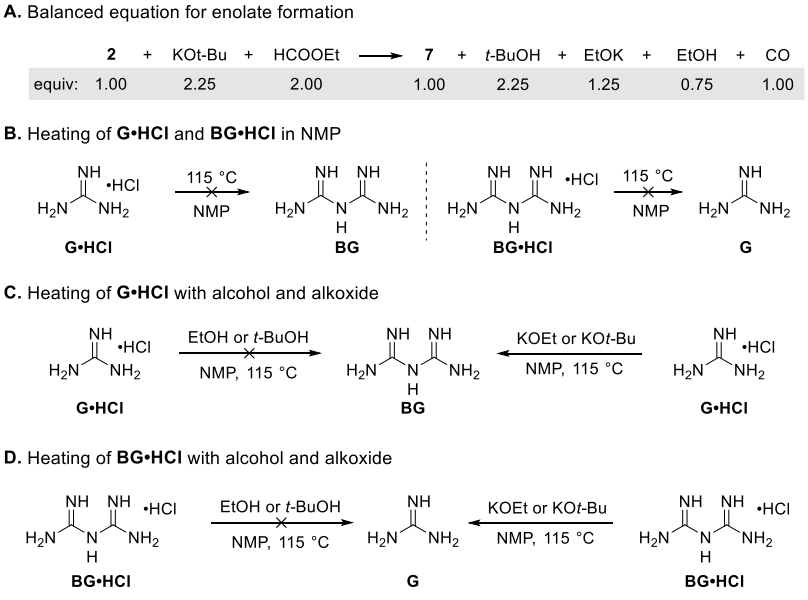

https://dx.doi.org/10.1021/acs.oprd.0c00246
Org. Process Res. Dev. XXXX, XXX, XXX−XXX

Scheme 10. Plausible Explanation of How Impurity 10 is Generated Based on ^{13}C-Labeling Experiments

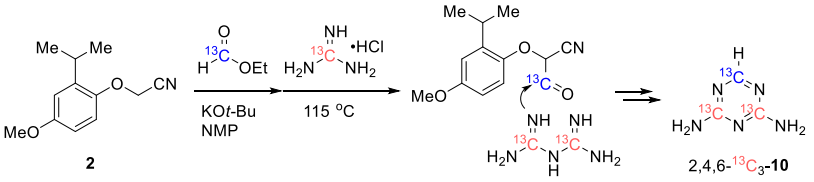

Scheme 11. Formation of Impurity 11 as Additional Evidence of Generating Biguanide *In Situ* during Enolate Cyclization with Guanidine Hydrochloride

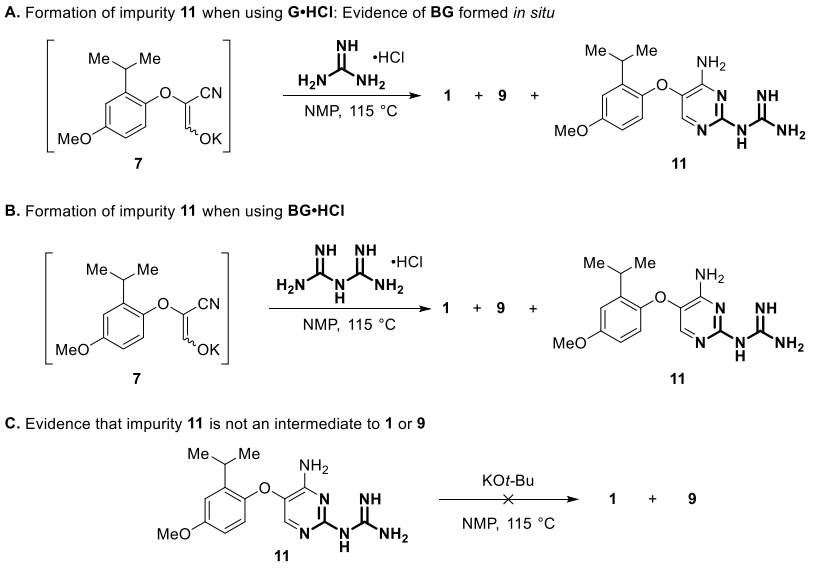

generate isourea, and the reaction of isourea with guanidine to generate biguanide are precedented in the literature.[10,11] The alkoxide-mediated dimerization of guanidine to form biguanide necessitates the release of NH_3 in order to balance the equation. Indeed, when the cyclization reaction was monitored by FT-IR, headspace analysis detected the presence of NH_3, specifically during the heating period after having added **G·HCl** to the enolate solution.

After establishing the root cause for the formation of biguanide, we returned to the question surrounding the loss of carbon originally derived from the carbonyl of ethyl formate toward the formation of triazine. Analysis of isolated **1** revealed the presence of 2,4-diamino-1,3,5-triazine (**10**) as an impurity. One potential route to form impurity **10** involves biguanide condensing onto the carbon subsequently lost during the cyclization step (Scheme 10). Furthermore, when ^{13}C-labeled ethyl formate and ^{13}C-labeled **G·HCl** were used for the enolate and cyclization steps, respectively, compound **10** containing ^{13}C isotopes at all three aromatic carbons was easily detected by NMR spectroscopy upon analysis of the EOR sample. Analysis of the reaction mixture by GC−mass spectrometry revealed a broad peak at 12−16 min associated with a m/z 112.0 when using ^{13}C-labeled ethyl formate, whereas this same GC-peak corresponded to m/z 111.0 when using unlabeled ethyl formate. These observations are consistent with the formation of compound **10** via incorporation of the carbon atom originating from ethyl formate. Because GC and *in situ* solution FT-IR analyses of the enolate formation revealed that no ethyl formate was detectable, the formation of impurity **10** must incorporate the carbon derived from enolate **7**, suggesting a deformylation pathway for the formation of triazine **10**. ^{13}C-labeled ethyl formate and ^{13}C-labeled **G·HCl** lead to triply ^{13}C-labeled 2,4-diamino-1,3,5-triazine (2,4,6-$^{13}C_3$-**10**), suggesting that **10** incorporates the formate carbonyl carbon atom.

Further analysis of isolated **1** revealed the presence of the unique impurity **11**, as shown in Scheme 11A. Isolation of this impurity and characterization via NMR spectroscopy unambiguously supports its structure, representing additional evidence in favor of the biguanide species generated during the cyclization reaction. This particular impurity was also observed when reacting enolate with biguanide hydrochloride directly (Scheme 11B). Attempts at converting impurity **11** under basic conditions (Scheme 11C), mimicking the cyclization process afforded neither triazine **9** nor compound **1**, which is consistent with impurity **11** not being an intermediate on the reaction pathway to either pyrimidine **1** or **9**. Finally when compound **1** was heated with **G·HCl**, no formation of **11** was observed.

Screening of Acid Additives. Based on our mechanistic insight that the excess alkoxide present in the enolate solution causes guanidine to convert, in part, into biguanide under the reaction conditions, we sought to utilize an acid additive to mitigate this competing pathway.[20] Specifically, addition of an acid additive prior to the cyclization event would quench the excess alkoxide and thereby suppress the formation of biguanide.[21] A screen of additives was undertaken to identify conditions to meet our goal of employing only 2−3 equiv of **G·HCl** for the cyclization reaction for 15 h, as opposed to 8 equiv. As shown in Table 5, cyclization reactions in the presence of 0.5 equiv of carboxylic acids, such as acetic acid, trifluoroacetic acid, and pivalic acid (entries 2, 3, and 4), decreased the amount of triazine to less than 3 area % compared 6.6 area % without an additive (entry 1). On the other hand, inorganic acids (entries 5

https://dx.doi.org/10.1021/acs.oprd.0c00246
Org. Process Res. Dev. XXXX, XXX, XXX−XXX

Table 5. Table of Additives Screened in Attempt to Suppress Formation of Impurity 9 in the Cyclization Step to Product 1

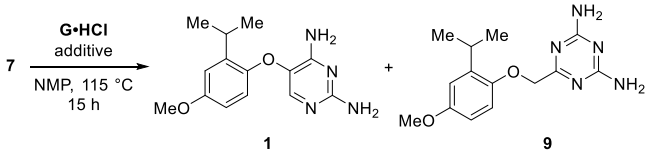

entry	G•HCl (equiv)	additive	1 (LCAP)	9 (LCAP)
1	3	none	87.2	6.6
2	3	MeCOOH (0.5 equiv)	91.3	1.5
3	3	CF_3COOH (0.5 equiv)	90.8	1.9
4	3	Me_3CCOOH (0.5 equiv)	92.4	1.3
5	3	conc. HCl (0.5 equiv)	75.0	0.9
6	3	H_2SO_4 (1.0 equiv)	26.0	7.0
7	3	$KHSO_4$ (0.5 equiv)	90.1	1.0
8	3	K_3PO_4 (0.5 equiv)	77.9	8.2
9	3	K_2HPO_4 (0.5 equiv)	86.5	3.2
10	3	KH_2PO_4 (0.5 equiv)	86.6	4.0
11	3	NH_4COOH (0.5 equiv)	87.6	0.5
12	3	NH_4ClO_4 (0.5 equiv)	87.0	1.0
13	3	$NH_4SO_3CF_3$ (0.5 equiv)	87.2	0.8
14	3	NH_4Cl (0.5 equiv)	89.2	0.9
15	3	NH_4Cl (0.75 equiv)	89.7	1.4
16	4	NH_4Cl (0.75 equiv)	92.7	1.0
17	5	NH_4Cl (0.75 equiv)	94.2	0.8
18	5	$(NH_4)_2SO_4$ (0.75 equiv)	80.6	1.7
19	5	$(NH_4)_2CO_3$ (0.75 equiv)	92.9	1.7

and 6) proved detrimental to the overall reaction profile. While use of 0.5 equiv of $KHSO_4$ (entry 7) showed promise, other salts, including potassium phosphate salts (entry 8−10), failed to provide any advantage. The cyclization reactions were also screened in the presence of ammonium salts (entries 11−14 and 18−19) and found to be equally efficient with regard to the reaction profile and controlling triazine formation under 2 area %. Ammonium chloride was selected for further screening and development work because it had the lowest price and greatest availability at a commercial scale. We were pleased to find that excellent results were achieved by further adjusting the amount of **G•HCl** and ammonium chloride (entries 14−17).

While analysis of the reaction mixtures at the end of cyclization seemed encouraging, this strategy led to several issues upon scale-up including lower and inconsistent isolated yields (77−84%) on a laboratory scale (ca. 5−15 g), a dark color of isolated **1** and the appearance of two solvent-related impurities **14a** and **14b** (Scheme 12), which were identified in the isolated solid at variable amounts with upward 1.5 area %, exhibiting poor rejection not only during the isolation of compound **1** but also in the downstream.

Notably, the appearance of the NMP moiety only on the C-2 amino group is intriguing (labeling of the C-2 position in **14a** & **14b** is shown in Scheme 12). We hypothesized that, under the basic conditions employed, NMP also undergoes formylation[22] to form enolate **12**, which generates the modified guanidine species **13** upon reaction with guanidine. Cyclization of compound **13** with enolate produces **14a−b** and explains the appearance of the NMP moiety only at the C-2 amino group. To validate the mechanism, we ran the reaction with ^{13}C-labeled ethyl formate, generating both impurities $^{13}C_2$-**14a** and $^{13}C_2$-**14b**, each containing two ^{13}C labels, as determined by mass spectrometry experiments on EOR mixtures. Quenching of an aliquot of the enolate reaction mixture and subsequent analysis by GC−MS revealed mass signals consistent with NMP-aldehyde **12b** and ^{13}C-**12b**, depending on whether ethyl formate

Scheme 12. (A) Proposed Rationale for the Generation of Impurities 14a and 14b; (B) Use of ^{13}C-Labeled Ethyl Formate Results in 14a and 14b Containing Two ^{13}C-Atoms as Determined by MS Analysis

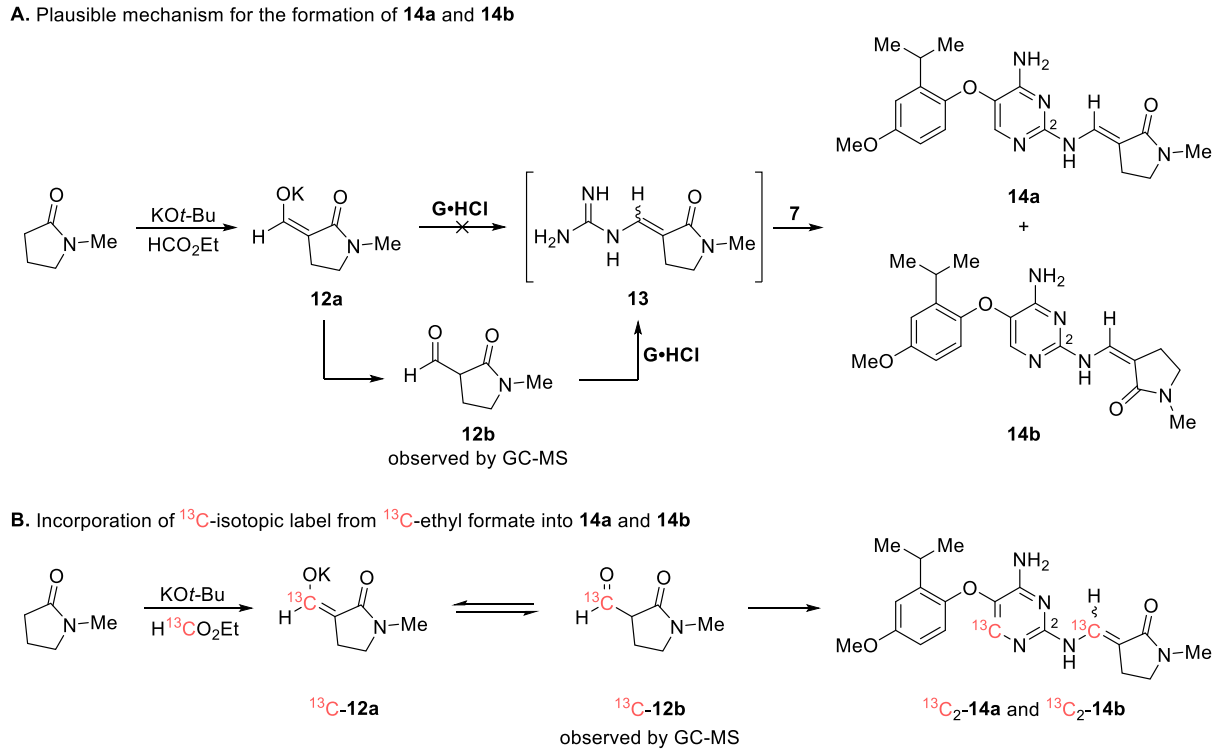

https://dx.doi.org/10.1021/acs.oprd.0c00246
Org. Process Res. Dev. XXXX, XXX, XXX−XXX

was unlabeled or ^{13}C-labeled, respectively (Scheme 12). It is worth noting that these impurities were also detected in the reactions employing 8.0 equiv of guanidine, albeit in <0.05 HPLC area %, as determined by the HPLC analysis of the reaction mixture. Discouraged by the finding of these elevated levels of solvent-related impurities in the presence of additives, we decided to carry out the cyclization reaction with 8.0 equiv of **G·HCl** for the long-term manufacturing process because of excellent yield and the consistent purity profile for compound **1**.

Isolation of Product 1. After accomplishing the synthesis of compound **1** with a high degree of control in an easily operable and one-pot sequence, we sought to effect a direct isolation employing an efficient crystallization process. The choice of NMP as the reaction solvent provided an ideal opportunity to directly isolate the desired product from water. During the cyclization reaction, the physical properties of the process stream changed from a solution to a thick slurry. We quickly discovered that the thick reaction mixture turned into a homogeneous solution during the addition of the water while maintaining the internal reaction temperature above 90 °C. With this information in hand, we decided to optimize the solvent system with an emphasis on designing a high-yielding crystallization process.

An extensive polymorph screen identified only one non-solvated crystalline form and an NMP-solvate of compound **1**. No hydrates were identified from the polymorph screen, and the nonsolvated form is thermodynamically stable at ambient conditions. Because residual NMP is undesired in the downstream chemistry, it was necessary to directly isolate the nonsolvated form. A phase map (Figure 3) was generated to

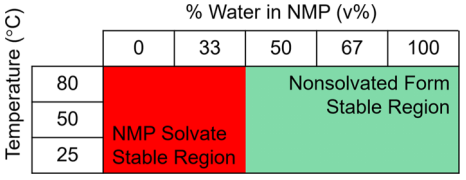

Figure 3. Phase map for product **3**.

understand the relative stability of forms as a function of temperature and solvent composition. From 25 to 80 °C, the NMP solvate is thermodynamically stable at water levels below 33 vol % in NMP, while at higher water content, the nonsolvated form can be generated. A suitable seeding point at 80 °C was identified that would allow us to crystallize the desired form.

To simplify the operation, the isolation process was carried out by charging all water (twice the volume of NMP), seeding at 82−87 °C, followed by cooling to 15−20 °C, and aging for 10 h. After filtration, the solid was washed with a mixture of 2:1 water/NMP (v/v), followed by water, to afford a wet cake that was dried under vacuum at 50 °C to afford diaminopyrimidine **1** in the desired form as an off-white solid. Remaining impurities present in the dry cake exhibited excellent rejection in the downstream chemistry, obviating the need for a further purity upgrade at this stage.

Incorporating all the previous optimization efforts, we were able to develop a robust process, as shown in Scheme 13. All impurities generated in this step were controlled within acceptable limits; in particular, compounds **8b** and **9** were limited to <1.5 and 0.15 area % in the final isolated solid. The final optimized process has been successfully implemented on a commercial scale to prepare approximately 2 metric tons of

Scheme 13. Optimized Process for Converting CME 2 to Product 1

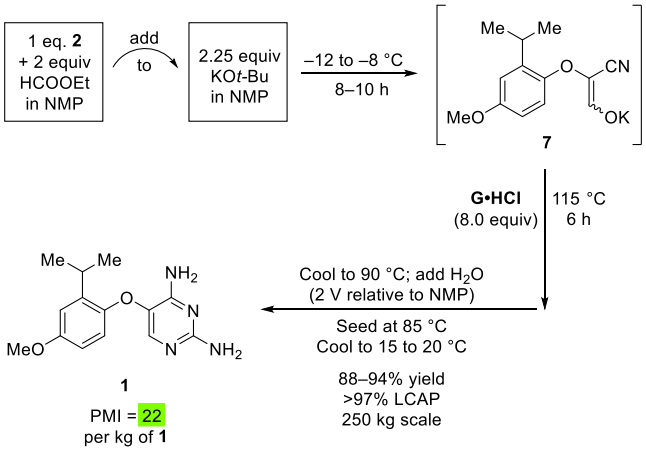

compound **1** in 88−94% isolated yield and >97% HPLC purity, as shown in Table 6.

Table 6. Tabulated Scale-Up Data for the Synthesis of Diaminopyrimidine 1

amount of **2** used (kg)	amount of **1** made (yield[a])	purity of **1** (LCAP)
280	375 kg (89%)	97.8
281	377 kg (88%)	97.7
281	352 kg (92%)	97.8
280	355 kg (92%)	97.2
280	362 kg (94%)	97.6
224	270 kg (89%)	97.4

[a]Isolated yield corrected based on the weight percent of the isolated material.

CONCLUSIONS

We have described the development of a robust and efficient synthesis of advanced intermediate **1** for the preparation of gefapixant citrate (MK-7264). The one-pot procedurally simple sequence entails an enolate formation, a cyclization, and a direct isolation. Key accomplishments include: (1) reduced cost by using ethyl formate, potassium *tert*-butoxide, and guanidine hydrochloride as reagents ($237 vs $2172 per kg of pyrimidine **1** as per Sigma-Aldrich pricing); (2) improved yield (88−94% vs 65%); (3) reduced PMI (step-PMI 29 vs 88 normalized to 1 kg of **1**); (4) shortened cycle time (36 vs 96 h); (5) eliminated additional purifications by developing a robust crystallization; and (6) thorough mechanistic understanding of the cyclization reaction guided by isotopic labeling experiments, which ultimately revealed the establishment of an equilibrium between guanidine and biguanide under basic conditions and, thereby, explained the formation of triazine **9** and other impurities (Figure 4).

The mechanistic understanding also pointed to a path forward through the implementation of additives during the cyclization reaction, only to conclude that this is not possible as long as NMP is used as the solvent because of the generation of NMP-related impurities that are difficult to reject downstream. In the end, the decision to switch from a variable and unpredictable impurity profile to a high-yielding and robust process in the presence of 8.0 equiv of guanidine was made, and the choice was validated on a commercial scale. Ultimately, the usage of excess

https://dx.doi.org/10.1021/acs.oprd.0c00246
Org. Process Res. Dev. XXXX, XXX, XXX−XXX

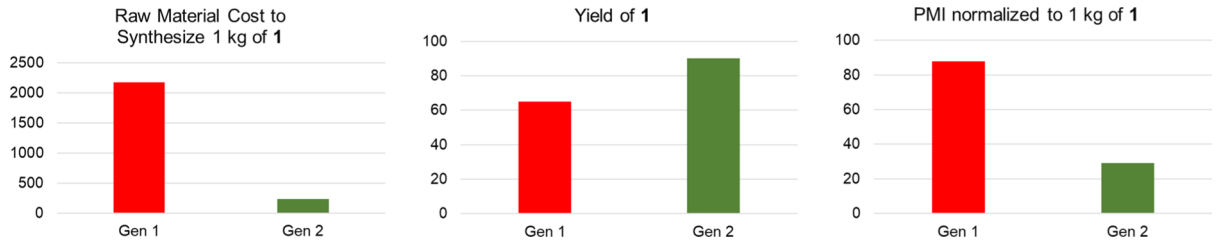

Figure 4. Graphical illustration of improvements in terms of: (left) raw material cost, (middle) yield, and (right) step-PMI normalized to 1 kg of **1** for the second generation (Gen 2) compared to the first generation (Gen 1) chemistry.

ethyl formate, potassium *tert*-butoxide, and guanidine was not a decision that was taken lightly, and revealed the limitations that are inherent to the way the batch process was carried out. The subsequent paper in this series[23] describes how this limitation with the improved batch process could be overcome by switching from the batch to flow mode for the enolate formation.

EXPERIMENTAL SECTION

Materials. Details below pertain to lab-scale development work. Reagents were purchased in the reagent grade from commercial suppliers and used without further purification, unless otherwise described. Anhydrous solvents (dimethylsulfoxide, *N*-methylpyrrolidine) were obtained from Sigma-Aldrich as part of their Sure/Seal bottles product line. NMR solvents, specifically, DMSO-d_6 (anhydrous, 99.9% *d*-content, catalog 570672-50G), CD_3CN (99.8% *d*-content, catalog DLM-21-10X0.75), and $CDCl_3$ (99.8% 99.8% *d*-content, catalog DLM-7-100) were purchased from Sigma-Aldrich and Cambridge Isotope Laboratories and used as received. UPLC-MS-grade acetonitrile (0.1 μm filtered) and UPLC-MS-grade water (0.03 μm filtered) were purchased from Thermo Fisher Scientific. Unless otherwise noted, all reactions were performed under an N_2-atmosphere.

Instrumentation. Proton nuclear magnetic resonance (^{1}H NMR) spectra and carbon nuclear magnetic resonance (^{13}C NMR) spectra were recorded at 25 °C (unless stated otherwise) on a Bruker 500 spectrometer using a liquid nitrogen-cooled triple resonance Prodigy CryoProbe or on a Bruker 600 spectrometer using a helium-cooled triple resonance CryoProbe. Chemical shifts for protons are reported in parts per million downfield from tetramethylsilane and are referenced to the residual proton of the NMR solvent according to values reported in the literature.[24] Chemical shifts for carbon are reported in parts per million (ppm, δ) downfield from tetramethylsilane and are referenced to the carbon resonances of the NMR solvent. For samples in $CDCl_3$, the residual solvent signal was referenced to 7.26 ppm for ^{1}H and 77.0 ppm for ^{13}C, for samples in CD_3CN the residual solvent signal was referenced to 1.94 ppm for ^{1}H and 1.32 ppm for ^{13}C, and for samples in DMSO-d_6, the residual solvent signal was referenced to 2.50 ppm for ^{1}H and 39.52 ppm for ^{13}C. Data are represented as follows: chemical shift, integration, multiplicity (br = broad, s = singlet, d = doublet, t = triplet, q = quartet, quint = quintet, hept = heptet, m = multiplet, dd = doublet of doublets, ddd = doublet of doublet of doublets, dt = doublet of triplets), coupling constants (J) in hertz (Hz). Homo- and heteronuclear coupling constants from the isotopic labeling experiments are specified as J_{CH}, J_{CC}, or J_{CN}. HRMS data were obtained using a Waters Acquity UPLC interfaced with a Waters Xevo G2 QTof ESI.

Manufacture of Diaminopyrimidine (1). Reactor 1 was charged with NMP (1119 kg), followed by KO*t*-Bu (277 kg, 2468.6 mol, 2.26 equiv) at 20 to 25 °C. The mixture was stirred for 1 h at 20 to 25 °C prior to cooling to −12 to −8 °C. A solution of CME **2** (224 kg, 1091.4 mol, 1.0 equiv) and ethylformate (110 kg, 2294.8 mol, 2.1 equiv) in NMP (102 kg) was charged to reactor 1, maintaining the internal temperature around −10 °C. The cold mixture was aged for 3 h when solid guanidine·HCl (834.1 kg, 8731.2 mol, 8.0 equiv) was charged to the reactor 1 followed by a NMP-flush (123 kg). The reactor was heated to 115 °C and aged for 6 h (<1% enolate by HPLC). The mixture was cooled to 90 to 95 °C when water (2370 kg) was added maintaining the internal temperature above 90 °C. The resulting homogeneous solution was cooled to 85 °C and seeded (1 wt % with respect to CME **2**, loaded as a slurry in 2:1 (v/v) H_2O/NMP). After being aged for 2 h at 85 °C, the slurry was linearly cooled to 15 to 20 °C over 6 h. The slurry was aged for additional 10 h, followed by filtration. The batch was filtered in an agitated filter dryer using Kavon 909 poly cloth. The wet cake was washed with 2:1 (v/v) water/NMP mixture (2 × 669 kg), water (2 × 669 kg) and dried under vacuum at 50 °C for ∼24 h to afford the desired diaminopyrimidine **1** as an off-white solid (270.4 kg, 89% yield, >97% purity). ^{1}H NMR (500 MHz, DMSO-d_6): δ 7.23 (s, 1H), 6.83 (d, J = 3.0 Hz, 1H), 6.70 (dd, J = 8.9, 3.0 Hz, 1H), 6.63 (d, J = 8.9 Hz, 1H), 6.32 (s, 2H), 5.75 (s, 2H), 3.71 (s, 3H), 3.28 (hept, J = 6.90 Hz, 1H), 1.20 (d, J = 6.9 Hz, 6H). ^{13}C NMR (126 MHz, DMSO-d_6): δ 159.64, 157.07, 154.96, 148.30, 144.06, 138.88, 130.28, 116.78, 112.45, 111.18, 55.30, 26.49, 22.75. ESI HRMS m/z: calcd for $C_{14}H_{19}N_4O_2$ ([M + H]$^+$), 275.1503; found, 275.1512.

*Spectral Data for 6-^{13}C-**1**.* ^{1}H NMR (500 MHz, DMSO-d_6): δ 7.23 (d, J_{CH} = 173.0 Hz, 1H), 6.83 (d, J = 3.0 Hz, 1H), 6.69 (dd, J = 8.9, 3.0 Hz, 1H), 6.62 (d, J = 8.9 Hz, 1H), 6.30 (br s, 2H), 5.74 (s, 2H), 3.71 (s, 3H), 3.28 (hept, J = 6.9 Hz, 1H), 1.20 (d, J = 6.9 Hz, 6H). ^{13}C NMR (126 MHz, DMSO-d_6): δ 159.72 (d, J_{CC} = 3.3 Hz), 157.04 (d, J_{CC} = 5.9 Hz), 154.93, 148.33, 144.26 (^{13}C enriched), 138.85, 130.21 (d, J = 74.1 Hz), 116.73, 112.44, 111.16, 55.29, 26.48, 22.74. ESI HRMS m/z: calcd for $^{13}C_1C_{13}H_{19}N_4O_2$ ([M + H]$^+$), 276.1536; found, 276.1539.

*Spectral Data for ^{15}N-**1**.* ^{1}H NMR (500 MHz, DMSO-d_6): δ 7.25 (s, 1H), 6.83 (d, J = 2.8 Hz, 1H), 6.70 (dd, J = 8.9, 2.9 Hz, 1H), 6.64 (d, J = 8.8 Hz, 1H), 6.22 (d, J = 87.5 Hz, 2H), 5.66 (s, 2H), 3.72 (s, 3H), 3.29 (hept, J = 6.9 Hz, 1H), 1.21 (d, J = 6.9 Hz, 6H). ^{13}C NMR (126 MHz, DMSO-d_6): δ 159.54 (d, J_{CN} = 2.6 Hz), 156.88 (d, J_{CN} = 20.1 Hz), 154.92, 148.17, 144.07, 138.78, 130.27 (d, J_{CN} = 1.8 Hz), 116.69, 112.40, 111.17, 55.22, 26.43, 22.58. ESI HRMS m/z: calcd for $C_{14}H_{19}{}^{15}N_1N_3O_2$ ([M + H]$^+$), 276.1473; found, 276.1475.

*Spectral Data for 2-^{13}C-**1**.* δ ^{1}H NMR (500 MHz, DMSO-d_6): δ 7.25 (d, J = 12.6 Hz, 1H), 6.83 (d, J = 2.9 Hz, 1H), 6.70 (dd, J = 8.9, 3.0 Hz, 1H), 6.64 (d, J = 8.8 Hz, 1H), 6.29 (br s, 2H), 5.65 (s, 2H), 3.72 (s, 3H), 3.28 (hept, J = 6.9 Hz, 1H), 1.21 (d, J = 6.9 Hz, 6H). ^{13}C NMR (126 MHz, DMSO-d_6): δ 159.54

https://dx.doi.org/10.1021/acs.oprd.0c00246
Org. Process Res. Dev. XXXX, XXX, XXX−XXX

(^{13}C-enriched), 156.89, 154.92, 148.17, 144.07 (d, J_{CC} = 3.5 Hz), 138.78, 130.28 (d, J_{CC} = 14.3 Hz), 116.69, 112.40, 111.18, 55.22, 26.43, 22.58. ESI HRMS m/z: calcd for $^{13}C_1C_{13}H_{18}N_4O_2$ (M^+), 275.1463; found, 275.1449. ESI HRMS m/z: calcd for $^{13}C_1C_{13}H_{19}N_4O_2$ ([M + H]$^+$), 276.1536; found, 276.1519.

Manufacture of CME (2). A 12 to 15 wt % solution of 2-isopropyl-4-methoxylphenol (314.3 kg, 12 wt %, 226.8 mol) was concentrated to 45 to 60 wt % 2-isopropyl-4-methoxyphenol in toluene under vacuum at 40 to 50 °C. To the solution was added 189 L of NMP, and the mixture was cooled to 5 °C. Sodium hydroxide (27.2 kg, 50 wt % in water, 340 mol) and chloroacetonitrile (36 kg, 340 mol) were added sequentially to the mixture while maintaining the internal temperature below 10 °C. The reaction was aged for 2 h and then diluted with 150 L of toluene and 226 L of water while maintaining the temperature below 10 °C. The mixture was warmed to 20 to 25 °C, the layers were separated, and the organic layer was washed with 75 L of 20 wt % NaCl (aq). The organic layer was concentrated to roughly two volumes and filtered to provide 2-(2-isopropyl-4-methoxyphenoxy)acetonitrile (56.8 kg, 74.6 wt %) as a solution in toluene. The filter was washed with NMP to provide additional 2-(2-isopropyl-4-methoxyphenoxy)acetonitrile (27.1 kg, 5.0 wt %) as a solution in NMP. The combined yield of **2** was about 94%. ^{1}H NMR (400 MHz, $CDCl_3$): δ 6.88 (d, J = 8.8 Hz, 1H), 6.83 (d, J = 2.9 Hz, 1H), 6.70 (dd, J = 8.8, 3.0 Hz, 1H), 4.72 (s, 2H), 3.79 (s, 3H), 3.27 (hept, J = 6.9 Hz, 1H), 1.22 (d, J = 6.9 Hz, 6H). ^{13}C NMR (126 MHz, $CDCl_3$): δ 155.82, 148.24, 140.13, 115.69, 114.27, 113.59, 110.61, 55.69, 55.30, 27.03, 22.98.

*Synthesis of ^{15}N-Labeled-**2**.* To a cold (0 °C), stirred solution of KO*t*-Bu (2.4 g, 21.7 mmol) in NMP (15.0 mL) was added a solution of 2-isopropyl-4-methoxyphenol (3.0 g, 18.1 mmol) in NMP (15.0 mL) over a period of 30 min. Neat chloromethyl methyl sulfide (2.1 g, 21.7 mmol) was added dropwise over a period of 15 min. The reaction mixture was slowly warmed to room temperature and aged overnight. The reaction was quenched with water (25 mL), followed by a saturated aqueous solution of NH_4Cl (25 mL). The resulting layer was extracted with heptane (2 × 25 mL). The combined organic layers were washed with 5 wt % aqueous solution of LiCl (20 mL), dried over $MgSO_4$, filtered, and concentrated to yield a residue that was purified by column on silica (elution with 100:1 to 10:1 hexane/EtOAc) to yield the desired thiomethylether intermediate as a colorless oil. ^{1}H NMR (500 MHz, $CDCl_3$): δ 6.85 (d, J = 8.8 Hz, 1H), 6.81 (d, J = 3.1 Hz, 1H), 6.67 (dd, J = 8.8, 3.1 Hz, 1H), 5.12 (s, 2H), 3.78 (s, 3H), 3.33 (hept, J = 6.9 Hz, 1H), 2.26 (s, 3H), 1.22 (d, J = 6.9 Hz, 6H). ^{13}C NMR (126 MHz, $CDCl_3$): δ 154.81, 148.41, 140.05, 114.94, 113.21, 110.31, 73.85, 55.70, 26.98, 23.05, 14.99. To a cold (0 °C), stirred solution of the above intermediate (1.5 g, 6.6 mmol) in DCM (6.0 mL) was added a solution of sulfuryl chloride (6.96 mL of 1.0 M solution in DCM, 6.96 mmol) dropwise. The resulting yellow solution was stirred at 0 °C for 1 h and then at room temperature for 30 min. The mixture was concentrated, and the residue was quickly filtered through a pad of silica, followed by washing with 30:1 hexane/EtOAc (100 mL). The filtrate was concentrated to provide the α-chloro ether. ^{1}H NMR (500 MHz, $CDCl_3$): δ 7.07 (d, J = 8.9 Hz, 1H), 6.82 (d, J = 3.1 Hz, 1H), 6.72 (dd, J = 8.9, 3.1 Hz, 1H), 5.89 (s, 2H), 3.79 (s, 3H), 3.29 (hept, J = 6.9 Hz, 1H), 1.20 (d, J = 6.9 Hz, 6H). This intermediate was dissolved in acetone (6.0 mL). To the solution was added K^{15}N (0.43 g, 6.6 mmol) and heated to 60 °C overnight. The resulting slurry was filtered and washed with MTBE. The filtrate was concentrated, and the residue was purified by column chromatography on silica gel (elution with 100:1 to 10:1 hexane/EtOAc) to afford the desired ^{15}N-labeled cyanomethylether (^{15}N-labeled-**2**) as a colorless oil. ^{1}H NMR (500 MHz, $CDCl_3$): δ 6.88 (d, J = 8.8 Hz, 1H), 6.85 (d, J = 3.1 Hz, 1H), 6.71 (dd, J = 8.8, 3.1 Hz, 1H), 4.71 (d, J_{NH} = 1.6 Hz, 2H), 3.79 (s, 3H), 3.29 (hept, J = 6.9 Hz, 1H), 1.23 (d, J = 7.0 Hz, 6H). ^{13}C NMR (126 MHz, $CDCl_3$): δ 155.68, 148.12, 139.96, 115.66 (d, J_{CN} = 16.1 Hz), 114.15, 113.44, 110.51, 55.54, 55.12 (d, J_{CN} = 2.9 Hz), 26.92, 22.85.

*Spectral Data for **8a**.* ^{1}H NMR (500 MHz, $CDCl_3$): δ 6.89 (d, J = 8.8 Hz, 1H), 6.85−6.81 (m, 3H), 6.72 (dd, J = 8.8, 3.1 Hz, 1H), 6.66 (dd, J = 8.8, 3.1 Hz, 1H), 4.84 (s, 2H), 4.68 (br s, 2H), 3.80 (s, 3H), 3.78 (s, 3H), 3.38−3.24 (m, 2H), 1.26−1.23 (m, 12H). ^{13}C NMR (126 MHz, $CDCl_3$): δ 155.97, 155.09, 148.80, 147.02, 145.44, 139.30, 139.10, 116.04, 115.29, 113.57, 113.36, 110.86, 110.48, 103.84, 77.41, 77.16, 76.91, 65.50, 55.75, 27.31, 27.22, 23.00, 22.99. ESI HRMS m/z: calcd for $C_{24}H_{31}N_2O_4$ ([M + H]$^+$), 411.2278; found, 411.2279.

*Spectral Data for **8b**.* ^{1}H NMR (500 MHz, DMSO-d_6): δ 6.80 (d, J = 8.9 Hz, 1H), 6.74 (d, J = 3.0 Hz, 1H), 6.64 (d, J = 3.1 Hz, 1H), 6.59 (dd, J = 7.0, 3.0 Hz, 1H), 6.58 (dd, J = 6.9, 3.1 Hz, 1H), 6.36 (d, J = 8.9 Hz, 1H), 6.27 (br s, 2H), 6.02 (s, 2H), 4.48 (s, 2H), 3.66 (s, 3H), 3.64 (s, 3H), 3.40−3.33 (m, 1H), 2.98−2.79 (m, 1H), 1.10 (d, J = 6.8 Hz, 6H), 0.98 (d, J = 7.0 Hz, 6H). ^{13}C NMR (126 MHz, DMSO-d_6): δ 160.06, 158.81, 154.22, 153.58, 149.84, 148.83, 138.01, 137.12, 125.61, 113.13, 112.61, 112.53, 112.33, 110.47, 110.19, 67.24, 55.30, 55.22, 26.22, 25.93, 22.67, 22.61. ESI HRMS m/z: calcd for $C_{25}H_{33}N_4O_4$ ([M + H]$^+$), 453.2496; found, 453.2483.

*Spectral Data for **9**.* ^{1}H NMR (500 MHz, DMSO-d_6): δ 6.89−6.60 (m, 7H), 4.64 (s, 2H), 3.67 (s, 3H), 3.33−3.25 (m, 1H), 1.15 (d, J = 6.9 Hz, 6H). ^{13}C NMR (126 MHz, DMSO-d_6): δ 173.61, 167.11, 153.59, 149.86, 137.90, 113.40, 112.42, 110.36, 71.42, 55.21, 26.19, 22.71. ESI HRMS m/z: calcd for $C_{14}H_{19}N_4O_2$ ([M + H]$^+$), 290.1612; found, 290.1616.

*Spectral Data for 2,4-$^{13}C_2$-**9**.* ^{1}H NMR (500 MHz, DMSO-d_6): δ 6.84−6.61 (m, 7H), 4.64 (s, 2H), 3.67 (s, 3H), 3.30 (hept, J = 6.94 Hz, 1H), 1.15 (d, J = 6.9 Hz, 6H). ^{13}C NMR (126 MHz, DMSO-d_6): δ 173.61 (t, J = 2.0 Hz), 167.09 (^{13}C enriched), 153.58, 149.86, 137.91, 113.41, 112.42, 110.35, 71.42 (t, J_{CC} = 5.1 Hz), 55.21, 26.20, 22.71. ESI HRMS m/z: calcd for $^{13}C_2C_{12}H_{19}N_4O_2$ ([M + H]$^+$), 292.1684; found, 292.1696.

*Spectral Data for **10**.* ^{1}H NMR (500 MHz, DMSO-d_6): δ 7.93 (s, 1H), 6.66 (br s, 4H). ^{13}C NMR (126 MHz, DMSO-d_6): δ 166.53, 166.03. GC LRMS m/z: calcd for $C_3H_5N_5$ (M^+), 111.0; found, 111.0.

*Spectral Data for **11**.* ^{1}H NMR (600 MHz, DMSO-d_6): δ 10.53 (br s, 1H), 8.41 (br s, 4H), 7.64 (br s, 1H), 7.39 (br s, 1H), 7.28 (s, 1H), 6.89 (d, J = 3.1 Hz, 1H), 6.88 (d, J = 8.8 Hz, 1H), 6.77 (dd, J = 8.9, 3.0 Hz, 1H), 3.74 (s, 3H), 3.13 (hept, J = 6.9 Hz, 1H), 1.17 (d, J = 6.9 Hz, 6H). ^{13}C NMR (151 MHz, DMSO-d_6): δ 156.34, 156.21, 155.50, 151.41, 145.88, 140.27, 138.79, 135.45, 119.75, 112.65, 111.82, 55.35, 26.65, 22.84. ESI HRMS m/z: calcd for $C_{15}H_{21}N_6O_2$ ([M + H]$^+$), 317.1721; found, 317.1721.

*Spectral Data for **14a**.* ^{1}H NMR (500 MHz, DMSO-d_6): δ 9.00 (d, J = 12.0 Hz, 1H), 7.78 (dt, J = 11.9, 2.5 Hz, 1H), 7.31 (s, 1H), 6.92−6.85 (m, 2H), 6.86 (d, J = 2.7 Hz, 1H), 6.78−6.71 (m, 2H), 3.73 (s, 3H), 3.35−3.29 (m, 2H), 3.22 (hept, J = 6.9 Hz, 1H), 2.76 (s, 3H), 2.65 (ddd, J = 7.7, 6.3, 2.5 Hz, 2H), 1.19 (d, J = 6.9 Hz, 6H). ^{13}C NMR (126 MHz, DMSO-d_6): δ 169.49, 156.91, 155.55, 154.15, 147.28, 142.01, 139.64, 133.23, 127.41,

https://dx.doi.org/10.1021/acs.oprd.0c00246
Org. Process Res. Dev. XXXX, XXX, XXX−XXX

118.31, 112.54, 111.49, 105.85, 55.31, 46.00, 29.42, 26.55, 22.82, 20.88. ESI HRMS m/z: calcd for $C_{20}H_{26}N_5O_3$ ($[M + H]^+$), 384.2030; found, 384.2020.

Spectral Data for ***14b***. ^{1}H NMR (500 MHz, DMSO-d_6): δ 9.76 (d, J = 11.2 Hz, 1H), 7.35 (dt, J = 11.1, 1.9 Hz, 1H), 7.28 (s, 1H), 6.94−6.86 (m, 2H), 6.86 (dd, J = 2.3, 1.2 Hz, 1H), 6.75−6.71 (m, 2H), 3.72 (s, 3H), 3.37 (dd, J = 7.7, 6.5 Hz, 2H), 3.21 (hept, J = 6.9 Hz, 1H), 2.76 (s, 3H), 2.65 (ddd, J = 8.2, 6.5, 1.9 Hz, 2H), 1.19 (d, J = 6.9 Hz, 6H). ^{13}C NMR (126 MHz, DMSO-d_6): δ 170.53, 157.16, 155.54, 152.86, 147.28, 142.05, 139.59, 133.27, 129.02, 118.17, 112.54, 111.48, 103.23, 55.31, 46.94, 29.15, 26.54, 22.81, 21.33. ESI HRMS m/z: calcd for $C_{20}H_{26}N_5O_3$ ($[M + H]^+$), 384.2030; found, 384.2023.

■ ASSOCIATED CONTENT

Supporting Information

The Supporting Information is available free of charge at https://pubs.acs.org/doi/10.1021/acs.oprd.0c00246.

NMR spectra, computational methods, and Cartesian coordinates of computed structures (PDF)

■ AUTHOR INFORMATION

Corresponding Authors

Kallol Basu − *Department of Process Research and Development, Merck & Co., Inc., Rahway, New Jersey 07065, United States;* orcid.org/0000-0002-4784-6068; Email: kallol.basu@merck.com

Dan Lehnherr − *Department of Process Research and Development, Merck & Co., Inc., Rahway, New Jersey 07065, United States;* orcid.org/0000-0001-8392-1208; Email: dan.lehnnherr@merck.com

Authors

Gary E. Martin − *Structure Elucidation Group, Analytical Research and Development, Merck & Co., Inc., Rahway, New Jersey 07065, United States;* orcid.org/0000-0003-0750-3041

Richard A. Desmond − *Department of Process Research and Development, Merck & Co., Inc., Rahway, New Jersey 07065, United States*

Yu-hong Lam − *Computational and Structural Chemistry, Merck & Co., Inc., Rahway, New Jersey 07065, United States;* orcid.org/0000-0002-4946-1487

Feng Peng − *Department of Process Research and Development, Merck & Co., Inc., Rahway, New Jersey 07065, United States;* orcid.org/0000-0002-2382-2862

John Y. L. Chung − *Department of Process Research and Development, Merck & Co., Inc., Rahway, New Jersey 07065, United States;* orcid.org/0000-0001-6094-5549

Rebecca A. Arvary − *Department of Process Research and Development, Merck & Co., Inc., Rahway, New Jersey 07065, United States*

Michael A. Zompa − *Department of Process Research and Development, Merck & Co., Inc., Rahway, New Jersey 07065, United States*

Si-Wei Zhang − *Department of Process Research and Development, Merck & Co., Inc., Rahway, New Jersey 07065, United States;* orcid.org/0000-0001-8677-3722

Jinchu Liu − *Department of Process Research and Development, Merck & Co., Inc., Rahway, New Jersey 07065, United States*

Zachary E. X. Dance − *Data Rich Measurements, Analytical Research and Development, Merck & Co., Inc., Rahway, New Jersey 07065, United States;* orcid.org/0000-0003-1807-7930

Patrick Larpent − *Department of Process Research and Development, Merck & Co., Inc., Rahway, New Jersey 07065, United States*

Ryan D. Cohen − *Structure Elucidation Group, Analytical Research and Development, Merck & Co., Inc., Rahway, New Jersey 07065, United States;* orcid.org/0000-0002-3112-6410

Francisco J. Guzman − *Department of Process Research and Development, Merck & Co., Inc., Rahway, New Jersey 07065, United States*

Nicholas J. Rogus − *Department of Process Research and Development, Merck & Co., Inc., Rahway, New Jersey 07065, United States*

Michael J. Di Maso − *Department of Process Research and Development, Merck & Co., Inc., Rahway, New Jersey 07065, United States;* orcid.org/0000-0003-1262-6126

Hong Ren − *Department of Process Research and Development, Merck & Co., Inc., Rahway, New Jersey 07065, United States;* orcid.org/0000-0002-0754-7282

Kevin M. Maloney − *Department of Process Research and Development, Merck & Co., Inc., Rahway, New Jersey 07065, United States;* orcid.org/0000-0003-1422-5422

Complete contact information is available at: https://pubs.acs.org/10.1021/acs.oprd.0c00246

Author Contributions

The manuscript was written through contributions of all authors. All authors have given approval to the final version of the manuscript.

Notes

The authors declare no competing financial interest.

■ ACKNOWLEDGMENTS

We would like to thank Louis-Charles Campeau, Rebecca Ruck, Eric Ashley, Guy Humphrey, Artis Klapars, and Christopher Nawrat (all at Merck & Co., Inc.) for providing insightful feedback on the manuscript and acknowledge Feiyue Wu, Peter Dormer, and Wilfredo Pinto for experimental contributions.

■ ABBREVIATIONS

DMF, *N*,*N*-dimethylformamide; DMSO, dimethylsulfoxide; EOR, end of reaction; ESI, electrospray ionization; EtOAc, ethyl acetate; GC, gas chromatography; HPLC, high-performance liquid chromatography; HR, high resolution; LC, liquid chromatography; LR, low resolution; MeCN, acetonitrile; MS, mass spectrometry; NMP, *N*-methyl-2-pyrrolidone; QToF, quadrupole time of flight; RMSD, root mean square deviation; RT, room temperature (ca. 25 °C); UPLC, ultraperformance liquid chromatography; δ, parts per million (ppm)

■ REFERENCES

(1) (a) Abdulqawi, R.; Dockry, R.; Holt, K.; Layton, G.; McCarthy, B. G.; Ford, A. P.; Smith, J. A. P2X3 receptor antagonist (AF-219) in refractory chronic cough: a randomised, double-blind, placebo-controlled phase 2 study. *Lancet* **2015**, *385*, 1198−1205. (b) Lederer, D. J.; Martinez, F. J. Idiopathic Pulmonary Fibrosis. *N. Engl. J. Med.* **2018**, *378*, 1811−1823. (c) Wang, J.; Wang, Y.; Cui, W.-W.; Huang, Y.; Yang, Y.; Liu, Y.; Zhao, W.-S.; Cheng, X.-Y.; Sun, W.-S.; Cao, P.; Zhu, M. X.; Wang, R.; Hattori, M.; Yu, Y. Druggable negative allosteric site of P2X3 receptors. *Proc. Natl. Acad. Sci. U.S.A.* **2018**, *115*, 4939−4944. (d) Ryan, N. M.; Vertigan, A. E.; Birring, S. S. An update and systematic

review on drug therapies for the treatment of refractory chronic cough. *Expert Opin. Pharmacother.* **2018**, *19*, 687−711. (e) Marucci, G.; Dal Ben, D.; Buccioni, M.; Martí Navia, A.; Spinaci, A.; Volpini, R.; Lambertucci, C. Update on novel purinergic P2X3 and P2X2/3 receptor antagonists and their potential therapeutic applications. *Expert Opin. Ther. Pat.* **2019**, *29*, 943−963.

(2) (a) Dvorak, C. A.; Green, K. L.; Lee, G. R. Process for Synthesis of Phenoxy Diaminopyrimidine Derivatives. WO 2008040652 A1, 2008. (b) Dillon, M. P.; Du Bois, D. J.; Jahangir, A. Diaminopyrimidines as P2X3 and P2X2/3 Modulators. U.S. Patent 20,080,207,655 A1, 2008.

(3) For a review on the use of Bredereck's reagent and related reagents such as DMF−DMA, see: (a) Kantlehner, W.; Bowers, A. tert-Butoxybis(dimethylamino)methane. *Encyclopedia of Reagents for Organic Synthesis*; Wiley, 2007. (b) Kidjemet, D. N,N-Dimethylformamide Dimethyl Acetal. *Synlett* **2002**, 1741−1742. (c) Abu-Shanab, F. A.; Sherif, S. M.; Mousa, S. A. S. Dimethylformamide dimethyl acetal as a building block in heterocyclic synthesis. *J. Heterocycl. Chem.* **2009**, *46*, 801−827. (d) Janin, Y. L.; Huel, C.; Flad, G.; Thirot, S. Methyl Orthocarboxylates as Methylating Agents of Heterocycles. *Eur. J. Org. Chem.* **2002**, 1763−1769.

(4) Based on online prices found on February 20, 2020 from commercial suppliers of this reagent on 1 kg scale.

(5) We draw the reader's attention to the fact that PMI in the literature can be defined one of two ways in multistep synthesis: (1) a step-PMI is the mass of all the reagents & solvents needed to obtain 1 kg of the product for that step; or, (2) an alternative version of PMI is the mass of all the reagents & solvents needed to obtain 1 kg of the final product of the total synthesis (i.e., the active pharmaceutical ingredient).

(6) For the definition of PMI and discussions of the topic, see: (a) Li, J.; Simmons, E. M.; Eastgate, M. D. A data-driven strategy for predicting greenness scores, rationally comparing synthetic routes and benchmarking PMI outcomes for the synthesis of molecules in the pharmaceutical industry. *Green Chem.* **2017**, *19*, 127−139. (b) Andraos, J. Useful Tools for the Next Quarter Century of Green Chemistry Practice: A Dictionary of Terms and a Data Set of Parameters for High Value Industrial Commodity Chemicals. *ACS Sustainable Chem. Eng.* **2018**, *6*, 3206−3214.

(7) Peng, F.; Humphrey, G. R.; Maloney, K. M.; Lehnherr, D.; Weisel, M.; Lévesque, F.; Naber, J. R.; Brunskill, A. P. J.; Larpent, P.; Zhang, S.-W.; Lee, A. Y.; Arvary, R. A.; Lee, C. H.; Bishara, D.; Narsimhan, K.; Sirota, E.; Whittington, M. Development of a Green & Sustainable Manufacturing Process for Gefapixant Citrate (MK-7264) Part 2: Development of a Robust Process for Phenol Synthesis. *Org. Process Res. Dev.* **2020**, DOI: 10.1021/acs.oprd.0c00241.

(8) Heating mixture of base and DMSO is known to be a safety hazard, for discussion of this topic, see (and references therein): (a) Yang, Q.; Sheng, M.; Li, X.; Tucker, C.; Cespedes, S. V.; Webb, N. J.; Whiteker, G. T.; Yu, J. *Org. Process Res. Dev.* **2020**, *24*, 916. (b) Yang, Q.; Sheng, M.; Henkelis, J. J.; Tu, S.; Wiensch, E.; Zhang, H.; Zhang, Y.; Tucker, C.; Ejeh, D. E. Explosion Hazards of Sodium Hydride in Dimethyl Sulfoxide, N,N-Dimethylformamide, and N,N-Dimethylacetamide. *Org. Process Res. Dev.* **2019**, *23*, 2210−2217.

(9) NMP was identified as the optimal solvent for the downstream pyrimidine formation which guided our efforts for developing the alkylation in NMP with the aim of avoiding a solvent switch between the two steps.

(10) Ren, H.; Maloney, K. M.; Basu, K.; Di Maso, M. J.; Humphrey, G. R.; Peng, F.; Desmond, R. A.; Otte, D. A. L.; Alwedi, E.; Liu, W.; Zhang, S.-W.; Song, S.; Arvary, R. A.; Zompa, M. A.; Lehnherr, D.; Martin, G. E.; Chang, D.; Mohan, A. E.; Guzman, F. J.; Jellett, L.; Lee, A. Y.; Spencer, G.; Fisher, E. S.; Naber, J. R.; Lohani, S.; Ruck, R. T.; Campeau, L.-C. Development of a Green & Sustainable Manufacturing Process for Gefapixant Citrate (MK-7264) Part 1: Introduction and Process Overview. *Org. Process Res. Dev.* **2020**, DOI: 10.1021/acs.oprd.0c00248.

(11) The computations were performed at the M06-2X/def2-TZVPP//M06-2X/6-31G** level of theory (gas phase). For enamines **5a−e**, the *Z*-isomer is 1.3−2.8 kcal/mol more stable than the *E*-isomer. For details, see Supporting Information.

(12) Synthetic strategies to access diaminopyrimidines in the literature include S_NAr substitution of dichloropyrimidine or transition metal-catalyzed coupling with amine nucleophiles, or cyclization approaches using guanidine derivatives with appropriate electrophiles to form the pyrimidine core. For references on these approaches, see: (a) von Angerer, S. Product Class 12: Pyrimidines. *Science of Synthesis*; Thieme Chemistry, 2004; Vol. *16*, pp 379−572. (b) Bourriquen, F.; Bruneau-Voisine, A.; Jeandin, A.; Stihle, E.; Fantasia, S. Streamlined Synthesis of Diaminopyridines by Pd-Catalyzed Ammonia Coupling with Deactivated Amino-Chloropyridines. *Chem.—Eur. J.* **2019**, *25*, 9006−9011. (c) Wyss, P. C.; Gerber, P.; Hartman, P. G.; Hubschwerlen, C.; Locher, H.; Marty, H.-P.; Stahl, M. Novel Dihydrofolate Reductase Inhibitors. Structure-Based versus Diversity-Based Drug Library Design and High-Throughput Synthesis and Screening. *J. Med. Chem.* **2003**, *46*, 2304−2312. (d) McGowan, D.; Herschke, F.; Pauwels, F.; Stoops, B.; Last, S.; Pieters, S.; Scholliers, A.; Thoné, T.; Van Schoubroeck, B.; De Pooter, D.; Mostmans, W.; Khamlichi, M. D.; Embrechts, W.; Dhuyvetter, D.; Smyej, I.; Arnoult, E.; Demin, S.; Borghys, H.; Fanning, G.; Vlach, J.; Raboisson, P. Novel Pyrimidine Toll-like Receptor 7 and 8 Dual Agonists to Treat Hepatitis B Virus. *J. Med. Chem.* **2016**, *59*, 7936−7949. (e) Létinois, U.; Schütz, J.; Härter, R.; Stoll, R.; Huffschmidt, F.; Bonrath, W.; Karge, R. Lewis Acid-Catalyzed Synthesis of 4-Aminopyrimidines: A Scalable Industrial Process. *Org. Process Res. Dev.* **2013**, *17*, 427−431.

(13) (a) Hamaguchi, M.; Matsubara, H.; Nagai, T. Reaction of Vinylcarbenoids with Benzaldehydes: Formation of Vinylcarbonyl Ylides Followed by Ring Closure to Oxiranes and Dihydrofurans. *J. Org. Chem.* **2001**, *66*, 5395−5404. (b) Shen, H. C.; Taggart, A. K. P.; Wilsie, L. C.; Waters, M. G.; Hammond, M. L.; Tata, J. R.; Colletti, S. L. Discovery of pyrazolopyrimidines as the first class of allosteric agonists for the high affinity nicotinic acid receptor GPR109A. *Bioorg. Med. Chem. Lett.* **2008**, *18*, 4948−4951. (c) Kim, Y.; Kim, J.; Kim, S.; Ki, Y.; Seo, S. H.; Tae, J.; Ko, M. K.; Jang, H.-S.; Lim, E. J.; Song, C.; Cho, Y.; Koh, H.-Y.; Chong, Y.; Choo, I. H.; Keum, G.; Min, S.-J.; Choo, H. Novel thienopyrimidinones as mGluR1 antagonists. *Eur. J. Med. Chem.* **2014**, *85*, 629−637.

(14) For exotherms that are greater than 50 J/g one should ensure, at a minimum, that the process is carried out with at least 10 °C difference between the maximum temperature (the sum of the operating temperature and the adiabatic temperature increase) and the initiation temperature. In this example the operating temperature is −10 °C, the adiabatic temperature increase is 34 °C, therefore the maximum temperature could potentially be 24 °C, which would also be more than 10 °C away from the initiation temperature (122 °C).

(15) (a) Myers, A. G.; Harrington, P. M.; Kuo, E. Y. Enantioselective synthesis of the epoxy diyne core of neocarzinostatin chromophore. *J. Am. Chem. Soc.* **1991**, *113*, 694−695. (b) Powers, J. C.; Seidner, R.; Parsons, T. G. The cleavage of formyl groups by sodium hydride. *Tetrahedron Lett.* **1965**, *6*, 1713−1716.

(16) We also explored alternative formylating agents (e.g., isopropyl formate and *tert*-butyl formate) with the hope that they would provide more stability under the reaction condition and thereby slow down the CO evolution. While isopropyl formate did not provide any advantage in regard to stability, *tert*-butyl formate proved not reactive enough to generate enolate **7**, thus resulting into higher amount of CME dimer formation. Evaluation of other non-ester formylating agents (e.g. DMF, 4-morpholinecarboxaldehyde) proved fruitless due to their inertness under the reaction conditions.

(17) We have looked for evidence of formamide in the end of reaction mixture but have not detected it. The absence of formamide does not rule out its formation.

(18) Both the addition of alkoxides to guanidine to generate isourea and the reaction of isourea with guanidine to generate biguanide are precendented in the literature, see: (a) Wang, Z.; Huynh, H. K.; Han, B.; Krishnamurthy, R.; Eschenmoser, A. 2,6-Diamino-5,8-diaza-7,9-dicarba-purine1. *Org. Lett.* **2003**, *5*, 2067−2070. (b) Shirai, K.; Sugino, K. Notes- Cyanamide Derivatives. LVII. New Route for Preparation of Biguanide. *J. Org. Chem.* **1960**, *25*, 1045−1046. (c) Cox, E. H.;

https://dx.doi.org/10.1021/acs.oprd.0c00246
Org. Process Res. Dev. XXXX, XXX, XXX−XXX

Raymond, S. M. Arylsulfonyl Ureas. *J. Am. Chem. Soc.* **1941**, *63*, 300−301.

(19) An alternative pathway to generate biguanide could proceed via elimination of cyanamide from guanidine. A subsequent reaction of either the cyanamide with guanidine, or the reaction of cyanamide with an alcohol to generate isourea followed by displacement with guanidine could lead to biguanide. The reaction of cyanamide with alcohols to generate isoureas is precedented, see: (a) Armitage, I.; Fu, M.; Hicks, F.; Kattuboina, A.; Li, J. S. N.; McCarron, A.; Zhu, L. The Use of Chloroformamidine Hydrochloride as a Reagent for the Synthesis of Guanidines from Electron Deficient Aromatic Amines. *J. Heterocycl. Chem.* **2017**, *54*, 728−734. (b) Kurzer, F.; Lawson, A. Methylisourea Hydrochloride. *Org. Synth.* **1954**, *34*, 67−71. (c) Manos-Turvey, A.; Al-Ashtal, HA; Needham, PG; Hartline, CB; Prichard, MN; Wipf, P.; Brodsky, JL; Brodsky, J. L. Dihydropyrimidinones and -thiones with improved activity against human polyomavirus family members. *Bioorg. Med. Chem. Lett.* **2016**, *26*, 5087−5091. (d) Paden, J. H.; Martin, K. C.; Swain, R. C. Guanidine Nitrate from Dicyandiamide and Ammonium Nitrate by Pressure Reaction. *Ind. Eng. Chem.* **1947**, *39*, 952−958. (e) Stieglitz, J.; Mc Kee, R. H. Ueber Methylisoharnstoff. *Ber. Dtsch. Chem. Ges.* **1900**, *33*, 1517−1519.

(20) Controling the pH of the reaction during the cyclization was also hypothesized to be beneficial based on existing literature, see: Robertson, M. P.; Levy, M.; Miller, S. L. Prebiotic Synthesis of Diaminopyrimidine and Thiocytosine. *J. Mol. Evol.* **1996**, *43*, 543−550.

(21) Immediately after adding the guanidine hydrochloride to the enolate, the reaction mixture is heterogeneous. At that time, the amount of alkoxides in solution may still be in excess relative to the amount guanidine hydrochloride in solution. Therefore, biguanide formation can occur prior to the mixture reaching a temperature where it is homogenous and able to achieve complete acid−base equilibration.

(22) While the formylation of NMP is not precedented as far as we know, it is known that NMP can be deprotonated and the subsequent nucleophile can be trapped with electrophiles. 1-Methyl-2-pyrrolidinone; Trapencieris, P.; Pigza, J. A. *Encyclopedia of Reagents for Organic Synthesis*; Wiley, 2009.

(23) Otte, D. A. L.; Basu, K.; Jellett, L.; Whittington, M.; Spenser, G.; Burris, M.; Corcoran, E. B.; Stone, K.; Nappi, J.; Arvary, R. A.; Donoghue, D.; Ren, H.; Maloney, K. M.; Naber, J. R. Development of a Green & Sustainable Manufacturing Process for Gefapixant Citrate (MK-7264) Part 4: Formylation-Cyclization as a Flow-Batch Process Leads to Significant Improvements in Process Mass Intensity (PMI) and CO Generated versus the Batch-Batch Process. *Org. Process Res. Dev.* **2020**, DOI: 10.1021/acs.oprd.0c00252.

(24) Gottlieb, H. E.; Kotlyar, V.; Nudelman, A. NMR Chemical Shifts of Common Laboratory Solvents as Trace Impurities. *J. Org. Chem.* **1997**, *62*, 7512−7515. (b) Fulmer, G. R.; Miller, A. J. M.; Sherden, N. H.; Gottlieb, H. E.; Nudelman, A.; Stoltz, B. M.; Bercaw, J. E.; Goldberg, K. I. NMR Chemical Shifts of Trace Impurities: Common Laboratory Solvents, Organics, and Gases in Deuterated Solvents Relevant to the Organometallic Chemist. *Organometallics* **2010**, *29*, 2176−2179.

https://dx.doi.org/10.1021/acs.oprd.0c00246
Org. Process Res. Dev. XXXX, XXX, XXX−XXX